Research Square

Preprints are preliminary reports that have not undergone peer review.
They should not be considered conclusive, used to inform clinical practice,
or referenced by the media as validated information.

Kraken: A wirelessly controlled octopus-like hybrid robot utilizing stepper motors and fishing line artificial muscle for grasping underwater

Yara Almubarak
University of Texas at Dallas
Michelle Schmutz
University of Texas at Dallas
Miguel Perez
University of Texas at Dallas
Shrey Shah
University of Texas at Dallas
Yonas Tadesse (yonas.tadesse@utdallas.edu)
University of Texas at Dallas https://orcid.org/0000-0001-6606-7089

Regular Paper

Keywords: Kraken, robot, twisted and a coiled fishing line polymer muscle (TCP FL)

Posted Date: February 8th, 2021

DOI: https://doi.org/10.21203/rs.3.rs-186985/v1

License: This work is licensed under a Creative Commons Attribution 4.0 International License.
Read Full License

Version of Record: A version of this preprint was published at International Journal of Intelligent Robotics and Applications on February 2nd, 2022. See the published version at https://doi.org/10.1007/s41315-021-00219-7.

Kraken: A wirelessly controlled octopus-like hybrid robot utilizing stepper motors and fishing line artificial muscle for grasping underwater

Yara Almubarak[1], Michelle Schmutz[1], Miguel Perez[1], Shrey Shah[1], and Yonas Tadesse[1*]

Humanoid, Biorobotics and Smart Systems (HBS) Laboratory, Mechanical Engineering Department, Erik Jonsson School of Engineering and Computer Science, The University of Texas at Dallas, Richardson, TX, United States of America
*Corresponding Author: Yonas.tadesse@utdallas.edu

Abstract

Underwater exploration or inspection requires suitable robotic systems capable of maneuvering, manipulating objects, and operating untethered in complex environmental conditions. Traditional robots have been used to perform many tasks underwater. However, they have limited degrees of freedom, manipulation capabilities, portability, and have disruptive interactions with aquatic life. Research in soft robotics seeks to incorporate ideas of the natural flexibility and agility of aquatic species into man-made technologies to improve the current capabilities of robots using biomimetics. In this paper, we present a novel design, fabrication, and testing results of an underwater robot known as Kraken that has tentacles to mimic the arm movement of an octopus. To control the arm motion, Kraken utilizes a hybrid actuation technology consisting of stepper motors and twisted and a coiled fishing line polymer muscle (TCP_{FL}). TCPs are becoming one of the promising actuation technologies due to their high actuation stroke, high force, light weight, and low cost. We have studied different arm stiffness configurations of the tentacles tailored to operate in different modalities (curling, twisting, and bending), to control the shape of the tentacles and grasp irregular objects delicately. Kraken uses an onboard battery, a wireless programmable joystick, a buoyancy system for depth control, all housed in a three-layer 3D printed dome-like structure. Here, we present Kraken fully functioning underwater in an Olympic-size swimming pool using its servo actuated tentacles and other test results on the TCP_{FL} actuated tentacles in a laboratory setting. This is the first time that an embedded TCP_{FL} actuator within elastomer has been proposed for the tentacles of an octopus-like robot along with the performance of the structures. Further, as a case study, we showed the functionality of the robot in grasping objects underwater for field robotics applications.

1. Introduction

The field of robotics deals in large with inhospitable environments wherein it is either impossible or very difficult for a person to operate in. One such environment is the high-pressure aquatic environment in which human physiology makes it practically impossible for a person to operate in without the assistance of either robots or other machinery. In this environment, even robots have a hard time dealing with both the high-water pressure due to the water and the adaptability needed to deal with the myriad of obstacles present in an aquatic environment. The adaptability of a robot is mainly determined by the way it moves and actuates its functional parts, and for a robot intended to function and explore underwater, the adaptability is a significant factor. For the purposes of improving the adaptability of robots beyond that provided by typical motor driven actuation, research is being performed into different bioinspired robotics utilizing novel actuators or artificial muscles. Several actuation technologies have been studied for robotics application such as electromagnetic (EM), pneumatic (PM), hydraulic (HA), piezoelectric (PZT), shape memory alloy (SMA), dielectric elastomer (DE), electroactive polymers (EAPs), and their composite forms. None of the mentioned technologies meet all the requirements of bioinspired robots design and development. For example, conflicting properties such as low cost and high performance in stress, strain, energy density, life cycle, efficiency, and frequency are difficult to get in one actuation technology. However, tradeoffs have been made in the design and developments of many robots. Twisted and coiled polymer fishing line muscles have been first introduced in 2014 by Haines et al. [1] as a new class of smart materials. These artificial muscles contract or expand when heated depending on the way they are manufactured. These inexpensive actuators were presented to have a high actuation stroke up to 50%, while lifting heavy loads at 1 MPa, and offering a high energy density of 5.4 kW/kg. The application of TCP actuators such as fishing line (TCP_{FL}) and silver-coated (TCP_{Ag}) has a wide range of contributions especially in bio-inspired robotics. We have been designing and developing several robots in the last few years using these actuators, TCP_{Ag} [2-6] and TCP_{FL} [7,6]. The TCP actuators are inexpensive, easily replaceable, are being used in various harsh environments, and are fully functional when exposed in underwater environments[5,8]. We aimed to design and develop an octopus-like robot utilizing TCPs for the arms (tentacles) due to their benefits in soft robotics. Additionally, we used conventional motors to make a hybrid system for the tendon driven arms. Our approach in design is to try to mimic

an octopus to some extent, but not the entire anatomy and swimming principles of an octopus, instead adapting only the flexible tentacles, and test the basic motion characteristics in an underwater environment.

Unique biomimetic systems have been presented in recent years. A biohybrid skeletal joint system is presented that can bend up to 90° and perform pick up and drop off tasks [9]; also a similar approach is shown for jellyfish like robot [10]. A bioinspired dual stiffness origami gripper is presented in [11]. Many researchers have also presented soft, silicone skin embedded with actuators and sensors such as temperature sensors [12], force sensors [13], pressure sensors [14], and TCP_{Ag} muscles [2].
Underwater robots play a vital role in many exploratory expeditions. Many oceanic researchers and archeologists use robots to study deep water conditions (+1,000 ft), animals, and sunken histories. These robots can reach depths, withstand cold and harsh water temperatures (4°C to 1°C), and general conditions that a human is physically incapable of facing safely. In this regard, a unique robotic fish was developed based on a biomimetic fish. It is equipped with a camera, which allows for the recording of aquatic life in their natural habitat [15]. Another fish was developed that utilizes SMA wires for swimming [16]. A robotic jellyfish, Robojelly, was fabricated mimicking the features of the Aurelia Aurita jellyfish species that is actuated using shape memory alloys [17]. A free-swimming jellyfish like robot was shown recently by Frames et al. [18] using hydraulic actuation system. An inflatable soft pneumatic composite (SPC) actuators based jellyfish with payload was shown by Joshi et al.[19]. Recently, an SMA jellyfish (Kryptojelly) is presented with unique features such as ease of varying the actuator parameters within the system and also multidirectional swimming [8]. Poly-Saora robotic jellyfish is also presented as a swimming biomimetic robot actuated by TCP_{Ag} muscles [5].

An octopus found in nature can conform to many non-uniform shapes underwater, as its body is able to bend and flex in many degrees of freedom. The flexibility of its body also serves as a protective measure against predators. An octopus can bend and extend its tentacles, allowing it to easily maneuver on the sand at the bottom surface of the ocean [20]. The swimming maneuvers of an octopus consists of two steps. The first one is when the tentacles are spread apart (open, recovery stroke). The second is when the tentacles are quickly moved to close (power stroke). The power stroke allows for significant thrust, allowing the octopus to propel its body forward [21]. Some dynamic models of an octopus robotic system have been presented in [22,23]. A biological study on the behavior of the tentacle movement is presented in [24]. The prototype presented, PoseiDrone, is made of several equidistant arms with swimming abilities imparted by using jet propulsion. Each arm has its own crank-like actuator that can bend or extend the arm using a sequence of sucking and releasing of the water from the chamber allowing for maneuvering [25,26]. An OctopusGripper, is also presented by Festo Inc., with each gripper arm inspired by the shape of an octopus tentacle. The tentacles of the OctopusGripper contain suction abilities that can sustain large gripping force with a working pressure of 2 bar [27]. A fully soft robot was presented by Fras et al. [28], with arms made of a novel soft fluidic actuator capable of manipulation as well as movement such as turning and forward propulsion. The robot is completely soft with even the main body being composed of an elastomer.

Calisti et al. [29] has presented a robot that contains a silicone arm with embedded cables that were actuated by servo motors to mimic the bending of the biological octopus tentacle. They have demonstrated the use of the arm by grasping objects and a pushing-based locomotion. Additionally, a multi-arm wirelessly controlled swimming octopus robot is presented by Sfakiotakis et al. [30,23,22,31]. This robot was able to propel itself and swim in underwater at a speed of 0.26 body length/second driven by waterproof micro servomotors. It is also able to perform a turning maneuver using a sequence of actuation steps. The main body enclosure contains an empty cavity that can be filled with water, which is utilized to control the buoyancy of the robot. Moreover, another soft robotic arm inspired by an octopus tentacle is presented, which has embedded coiled SMAs. The arm can bend and manipulate objects. The arm is made of transverse coiled SMA muscles around a cylinder shape of the octopus arm [32,33]. An 8-arm octopus-like robot was fabricated and tested [34], which is neutrally buoyant. The robot was able to move underwater over different surfaces and physical constraints. It is also able to grasp objects of different shapes and sizes. The swimming and grasping are a result of using two different arm actuating units, the motor crank for locomotion and the coiled SMA technology for manipulation. More works inspired by the biological behavior of the octopus tentacle are researched such as the multilegged climbing robot described in [35], the soft robotic actuator presented in [36], and the magnetically actuated octopus-like robot developed in [37]. Moreover, a case study has been presented, which introduces the control of the morphology of an octopus tentacle [38]. A review paper presented by Kwak and Bae explored the possibility of utilizing the biomimetics of arthropods for underwater application [39]. Salazar et al.[40,41] has shown the review of underwater robots discussing several issues.

The Kraken is known as a legendary cephalopod-like sea monster. This creature is often portrayed in fiction as a "giant squid" that is very strong and able to swallow ships, whales, and any obstacle it may encounter. This squid like creature is able to stay submerged underwater for days [42]. Our octopus-like robot (**Fig.1**) was deliberately named Kraken to emphasize on the impact this research can reach by developing a strong, durable, functional biomimetic robot. The biomimetic angle of our robot lies more in the goal of attaining the flexibility and strength of an octopus found in nature rather than mimicking its exact physiological mechanisms. Our robot, Kraken weighs 9.52 kg (20 lb) with all its components, measures 0.5x0.25x0.25m (20x10x10in) in size and has 4 tentacles. We present the design and the prototype of the robot that is capable of operating underwater in a swimming pool 24x24x1.8m (80x80x6 ft). A hybrid actuation system is implemented to effectively actuate the octopus's tentacles in order to grasp objects underwater. Out of the four arms (tentacles), three of them are actuated using stepper motors and the fourth arm is actuated by TCP_{FL}. The key parameters of the Kraken robot are shown in Table 1 along with a brief comparison with other fully developed octopus-like robots.

The TCP_{FL} are twisted and coiled polymer (TCP) muscles constructed from fishing line (FL). These actuators are based on previously presented work from our group, which uses electrothermal actuation of the polymer-based muscle (nylon 6) and a heating wire (80 µm diameter nichrome)[7,6]. Our TCP_{FL} arm for the robot shows tremendous potential for the advancement in soft robotics as it occupies less physical space in the robot while still maintaining a considerable amount of strength for its size. The wireless configuration of the robot allows for increased maneuverability, especially in areas that exterior cables would otherwise become easily entangled in. Having such a robot will help elevate the underwater research and exploration by making it more cost-effective, safe, flexible, and reliable.

The aim of this study is to design, develop and investigate the behavior of a new hybrid octopus-like robot through experimental method and theory. The key objectives of this research are to: (1) Create a wirelessly controlled, untethered octopus-like robot that is capable of grasping objects underwater using hybrid actuation methods, namely a combination of an artificial muscle and stepper motors. The artificial muscles are recently discovered materials based on twisted and coiled nylon. (2) Investigate the actuation behavior of silicone arms consisting of tendons, metallic leaf springs, filler materials, for ultimate use in the robot. This initial multi-system hybrid design focuses on the mechanisms of the silicone arms. (3) Design and manufacturing of the robot using mainly additive manufacturing and maintaining low material cost, high flexibility in the arms, and light weight system. (4) Perform characterization experiments on the robot, and finally, identify the relationships of the input and output parameters of the silicone arm embedded with an artificial muscle.

We conceptualized the design by sketching the entire architecture and creating the refined CAD model, and we fabricated most of the components using 3D printing and casting the silicone arms. Our approach to meet the objectives was to actuate three of the robotic arms with stepper motors and one of the arms using the artificial muscle to help us compare them and identify practical issues. The robot is tested in both lab setting and outside (field test), and we tested the silicone arms with an embedded actuator individually as well.

Our design of Kraken is robust and consists of the following key features:

- A 3-D printed dome-like exterior that has a watertight seal over all the electronics and hardware of the robot as shown in **Fig.1,** which can swim along people as a co-robot and grasp objects. It has three cascaded layers, which are the actuation unit, buoyancy unit, and electronics unit.
- Six different soft flexible arm configurations (Type I to VI) offering multi-dimensional actuation options (curling, twisting, and bending) for grasping several objects shown in **Fig.4**. We used only four arms (Type II, IV, V and VI) in the robot but we can replace any of the six arms depending on the need.
- The inexpensive mandrel coiled TCP_{FL} actuators have high actuation(up to 50% strain[7]), moderate stress (> 1 MPa), are easy to fabricate in house, can conform to geometries and therefore suitable to use in bioinspired robots. Here, we used one self-coiled TCP_{FL} artificial muscle for the robot due to the high blocking force (800g) and moderate strain (30% strain at 300g load). Characterization of the actuator used in the robot is presented in **Fig.5.**
- A hybrid actuation technology is presented allowing for each of the soft silicone tentacles to be actuated using a stepper motor or TCP_{FL} actuator (**Fig.6).** A fishing line artificial muscle combined with stepper motors has not been demonstrated for octopus-like robot and this is the first demonstration.
- A buoyancy system consisting of an air bladder, CO_2 gas supply and valves are included in the robot, which allows vertical movement (floating and sinking) underwater upon inflation and deflation.
- A wireless joystick controller allows for complete hands-off control of the robot's lithium-ion battery powered electronic subsystems as shown in the field test conducted in **Fig.1** and **Fig.3.**

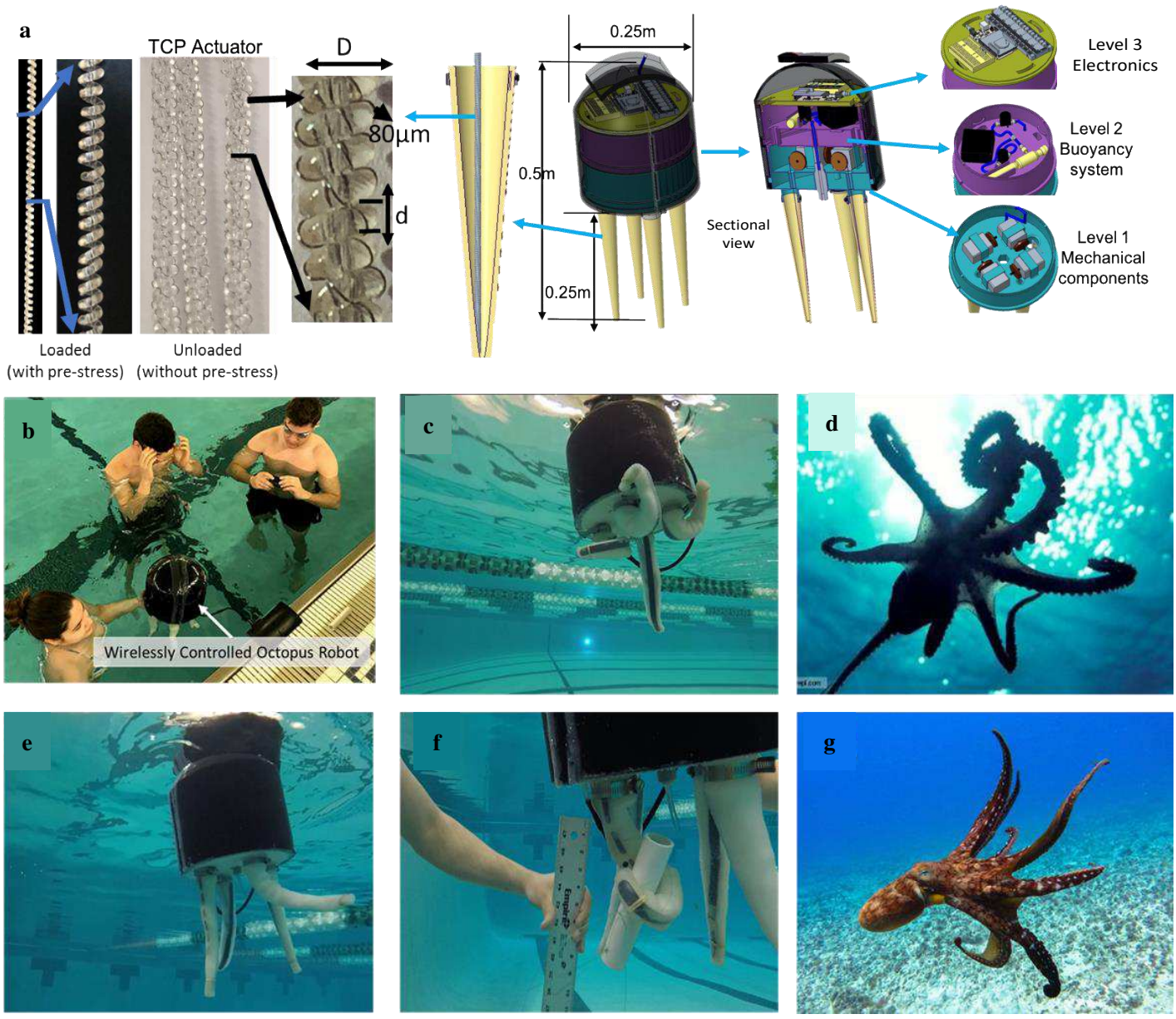

Fig. 1: Kraken hybrid robot for underwater grasping. a TCP fishing line actuator in loaded and unloaded conditions after annealing, diameter, D = 2.80 mm. The resistance wire is Nichrome (nickel and chromium) with diameter, dw=80 µm. CAD model showing the major components of the hybrid robot, b Kraken deployed in water, c Curling 3 arms, d Octopus found in nature with curling tentacles, e Floating on the surface, f Grasping PVC pipe underwater, g Natural octopus swimming.

Key aspects of our robots are compared with other robots in terms of actuation technology used, type of locomotion, type of control, biomimetic structure, overall dimensions, and the resulting manipulation capabilities in table 1. The unique combination of technologies, both novel actuators and traditional actuators used in our robot (**Fig.1a**), makes it a unique underwater preliminary probe capable of adapting easily to different situations and gathering valuable data before a more complete solution is determined. **Fig.1(b)** shows Kraken deployed in the water (**shown in movie 1, supplementary file**). **Fig.1(c-d)** show the octopus robot underwater and octopi found in nature with similar curling arm actuation. **Fig.1 (e-f)** show the different grasping angles of the arm actuating and utilizing the stepper motor actuated arms. We have shown controlling Kraken wirelessly in underwater conditions up to a depth of 6 feet (1.8m) as i**n movies 2 and 3**. Kraken is equipped with several arm stiffness configurations, which allows for the grasping of different objects, shapes, and orientations (shown in **Fig.4** and **movie 4**). The new technology of TCP actuators is used in one of its tentacles to assess the potential of grasping underwater. This was done to compare and contrast as well

as identify the basic characteristics of the two actuation systems in underwater conditions, because we don't know the behavior of the TCP embedded arm motion in response to different input conditions and geometry. Therefore, experiments are necessary to determine those variables and identify the basic science of actuation such as fluid mechanics, heat transfer kinetics and manipulation associated with the motion of the arms. The results presented are explained in different sections. First, we present different stiffness configurations for the silicone tentacles. Second, a characterization of the TCP_{FL} actuator is presented. Then, we show the implementation of the TCP_{FL} arm in air and in underwater conditions. Next, we show Kraken deployed in a swimming pool highlighting its wireless capabilities and onboard controlling system. Kraken can perform dexterous tasks such as grasping and vertical swimming (shown in movies 2 and 3). Finally, we show the flow analysis test results that were conducted to verify the design constraints and parameters of the robot.
Note that all supporting information and figures are provided in supplementary files and they are designed with "S" to differentiate with the main figures.

Table 1: Comparison of current full octopus-like robots with arm length greater than 0.2m

Name/ Category	Kraken (this paper)	PoseiDrone [25]	Octopus Inspired Multi-Arm Robotic Swimmer [31,22,23,30]	The Soft Eight-Arm OCTOPUS Robot [34]
Actuation Technology	• Four stepper motors with tendon • Twisted and coiled fishing line actuator TCP_{FL}	• Dyneema cables driven by servomotors	• Servomotors Hitech, HS 5086WP	• Motor driven tendons • Coiled shape memory alloys
Locomotion/ propulsion	• Vertical swimming using buoyancy system	• Crawling by pushing and pulling. • Swimming using a buoyancy module and pulsed jet.	• Swimming and turning using the movement of its arms.	• Able to crawl using push and pull strategies
Control	• Wirelessly controlled	• Controlled externally through a connecting wire.	• Controlled remotely through an RF connection.	• External communication
Sensors	• Temperature	• None	• None	• Contact sensors • Stretch sensors
Structure	• 3D printed housing composed of 3 levels • 4 soft silicone arms mounted on bottom level.	• Composed of six arms, a swimmer module and a buoyancy module.	• Eight arms mounted to a compliant housing with buoyancy and electronic systems.	• Eight arms mounted to a platform on which the motors are mounted.
Dimensions	• Weighs 9.52 kg • Arm length 0.25m (TCP is 110 mm) • Size 0.5x0.25x0.25 m	• 0.78 m long • 0.245 m per arm	• 0.2m arm length • 0.16m radius • Weighs 2.68 kg	• Arm length 0.3m
Manipulation	• Capable of grasping using stepper motor arms. Lifting weights using the TCP_{FL} arms	• Able to lift and hold items while moving.	• Able to grasp using multiple arms	• Two arms using SMA.
Powering / duration	• Lithium ion battery 4400 mAh. • 45 minutes swimming	• None	• Li-Po battery • 1 hour continuous operation	• None

2. Materials and Methods

As stated earlier, the objective of this research is to create a wirelessly controlled untethered octopus-like robot using a combination of artificial muscles and stepper motors. Here, we describe the materials used and the testing methods in both experimental and theoretical frameworks.

2.1. Twisted and coiled polymer (TCP_{FL}) fishing line muscle

Table 2: Fishing line TCP muscle information	
Material	Nylon (6,6) fishing line
Type of actuation	Electrothermal
Type of resistance wire	Nichrome (nickel, chromium)
Resistance wire diameter	d_w=80 µm
Precursor fiber diameter	d =0.8 mm
Length of precursor fiber	l = 1143 mm
Weight for fabrication	m_f = 500 g
Annealing Temperature/ Time	Ta=180^{0}C/ 90 min
Training protocol	According to figure S2 (c)
Diameter after coiling	D=2.8mm
Length after coiling	L=110 mm
Resistance	R= 256Ω
Current (Input)	I= 0.14A - 0.47A
Voltage (Output)	V= 35V - 120V
Input power (V*I)	P = 4.9W - 56.4W
Heating time(t_h)	t_h=25s - 1s
Cooling time (t_c)	t_c =100s - 9s
Heating energy(V*I*t_h)	E_h=122.5J - 56.4J
Actuation frequency	f = 8mHz – 0.1Hz
Actuation strain, at 300g load	ε = 40% - 10%
Blocking force (experimental)	~8N (800g) [6]

TCP muscles are artificial muscles made by using semi crystalline polymer precursor fibers by extremely twisting it under a constant load and then heat treating it. They are capable of contracting when heated and produce mechanical work. Artificial muscles such as TCP_{FL} can be controlled either by hydrothermal actuation or joule heating. In our case, Joule heating is the most ideal, as it eliminates the necessity to add complex water heating and cooling systems within the octopus robot structure. To introduce Joule heating into a material that is inherently nonconductive, several researchers have introduced electrical wires such as copper wires [43], and flexible carbon nano tubes sheets on to the twisted coils [1]. Wu et al [7], from our group, has introduced a novel method of wrapping nichrome resistance wire on to the fishing line fiber after twisting and before coiling. This specific method enables the use of thin nichrome wire of 80µm diameter. **Fig.1(a)** shows the structure of TCP muscles/actuators.

The small diameter has a minimal effect on the coiling process during fabrication and the mechanical performance of the actuator. Also, it allows for a more uniform temperature gradient throughout the muscle when heating. This ensures an even distribution of the temperature. We have followed very similar fabrication methods to our previous work presented in [6] to achieve high quality data on the actuator used in the robot arms. We created self-coiled structures that have high forces in this study. The complete properties of the actuator are found in **Table 2**. The TCP_{FL} has an actuation strain up to 40% using an electrothermal mode of actuation as presented in ref [6].

2.2. Fabrication of fishing line muscle with thin heating wire

The fabrication of the self-coiled fishing line muscle with heating element is simple, scalable, and easy to follow which allows for in-house manufacturing of the actuators at low cost. It consists of four major steps following [6] and shown in movie 9, explained in **Fig.S2(a)** [7,6]. First, twist insertion; second, wrapping of nichrome resistance wire; third, coiling; and fourth, thermal annealing and training. We attached a precursor fiber of fishing line muscle, purchased from Eagle Claw (0.8 mm in diameter and 1143 mm in length), to a motor (mounted on the top) and the other end to a 500g deadweight. The precursor fiber is twisted and then nichrome wire is incorporated as a heating element. This process is important to avoid breakage of the thin wire (80 µm). After that, the muscle is coiled; then crimped on both ends and annealed in a furnace at 180°C for 90 minutes to preserve its coiled shape. This annealing process aligns the crystal structure of the nylon, which allows it to stay at the coiled shape. **Fig.1 (a)** shows the self-coiled fishing line muscle after annealing with diameter of D = 2.80 mm and a length of 110 mm. Lastly, the muscle is trained at 300g load with multiple heating cycles following the protocol shown in **Fig.S2 (c)** to retain a certain actuation load. Thermal imaging of before (t = 0s) and during actuation (t = 5s) is shown in **Fig.S2(b).**

2.3. Isotonic testing of fishing line muscle

Isotonic testing of the actuator was done by hanging a calibrated weight (constant load) at the tip of the actuator. A square wave current input was applied to the muscle while data, such as actuation strain, temperature, and output voltage were collected and analyzed. **Fig. 5(a)** shows the schematics of the experimental setup. The set up contains the fishing line actuators, NI DAQ 9219, Keyence laser displacement sensor, thermocouples, LabVIEW program, power supply, and calibrated weights. **Fig.S3(a-c)** show the connection circuit. The test was conducted at three different current inputs of 0.2A, 0.3A, and 0.4A.

2.4. Fabrication of the silicone arm

A step by step process of creating one of the basic arms found on Kraken is presented in **Fig 2(a).** The process first starts out with the molding of the silicone arms. Using a flat 3D printed mold of the arm shape. Mann Ease Release 200 spray was applied throughout the surface of the mold to prevent sticking. EcoFlex 00-30 part A and B were mixed together at a 1:1 ratio and a small layer of silicone was poured into the mold. Silicone elastomer material (Ecoflex-0030) is used as an artificial skin material due to its elasticity and molding abilities. After mixing the silicone, the chosen arrangement of spring steels is added to the first layer of silicone. The specific arrangement and thickness of the spring steels will determine the shape the arm takes when actuated. This is explained further in the results and discussion section. Adding thin strips will cause the arm to bend at different axes. Also, depending on the angle of orientation that the spring steel is embedded with, we can achieve different curling configurations. After laying out the desired configuration, the rest of the silicone is then poured on top of the spring steel layer. To connect the arm to the stepper motor, a long piece of fishing line passive structure (used as tendon) is embedded into the bottom end of the silicone while it is still uncured. Once the silicone is cured, it is removed from the mold. Then, beginning from the base of the arm, the silicone is folded over the sides and the cap is sealed using small amounts of fast curing EcoFlex 00-35. Moreover, cotton was added inside the arm to increase the stiffness. A similar process is also implemented for the TCP_{FL} arm by placing the coiled fishing line muscle instead of the passive fiber before curing and folding the silicone.

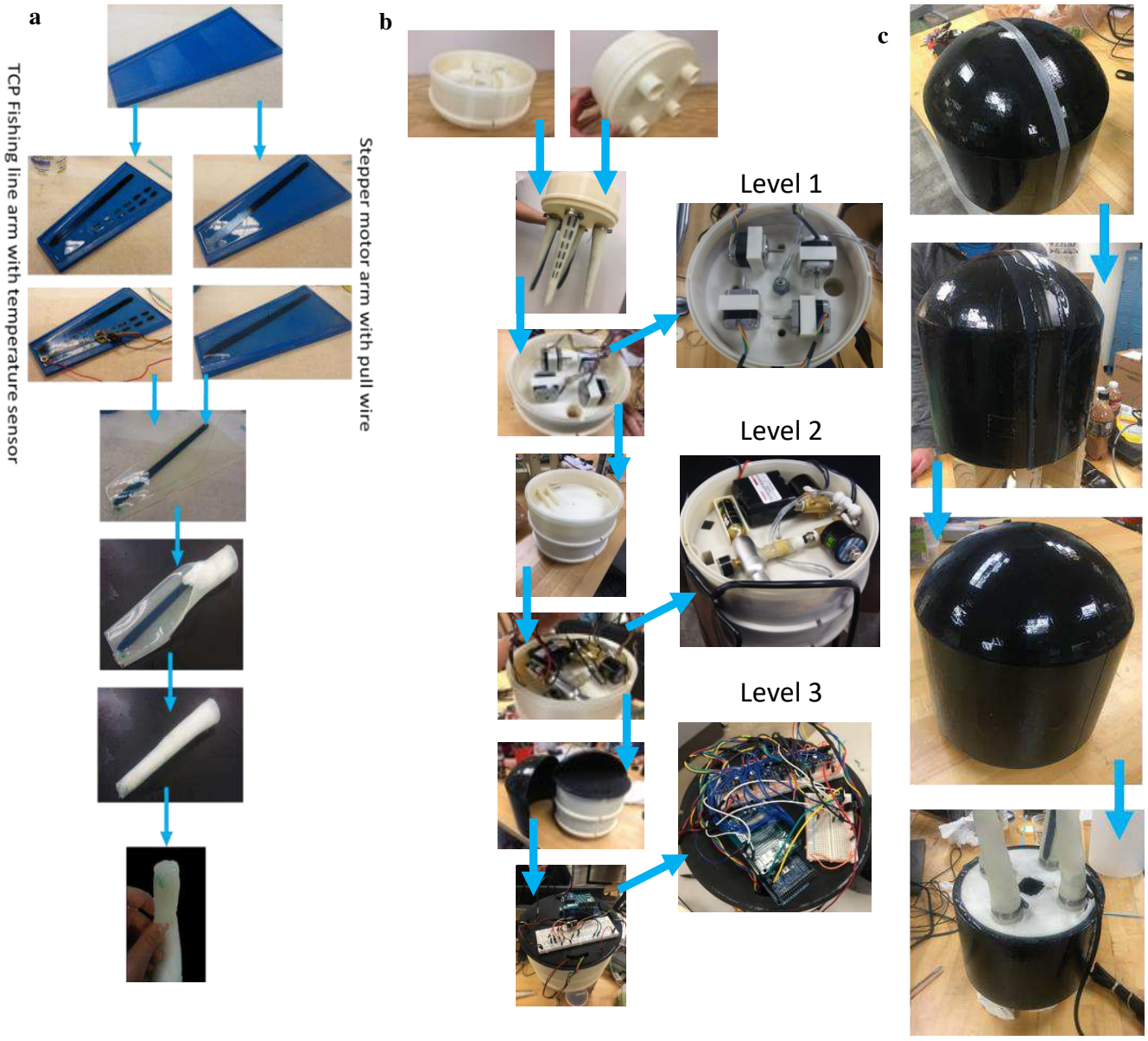

Fig. 2: Fabrication process (a) Silicone arm fabrication process, (b) 3D printed parts assembly, detailed view of the three internal levels, level 1stepper motors, level 2 buoyancy system, level 3 electrical circuit. (c) Water sealing process using FlexSeal paint.

2.5. Overall robot design and manufacturing (mechanical and electrical components)

The robot is divided into three levels as shown in **Fig.2(b)**. The first level contains the four 5.5 kg-cm bipolar NEMA 17 stepper motors and the TCP_{FL} actuator that control the soft silicone arms. The second level contains the buoyancy system, which is comprised of two solenoid valves, check valve, pressure regulator, air bladder, and a 16g CO_2 canister. Lastly, the third level contains the electrical controlling circuit, which includes the wireless communication module, a battery power source, an Arduino board, a voltage boost converter, and motor drivers. Due to the power and battery limitations, the integration of a voltage boost converter (GEREE 250W Boost Converter) to the circuit is essential for the actuation of the fishing line muscle for grasping. We have shown the actuating circuit and connectivity diagram **Fig.3(a-b)** for both the stepper motors and the TCP_{FL} using the boost converter to increase the voltage provided by the battery by decreasing the current output. Due to the actuator's high resistance (R= ~200-400 **Ω**), it takes low current (I = 0.12A-0.5A) but high voltage (V= 30V-150V), therefore, stepping down the current creates no

issues for this application. Detailed connection diagram of the circuit is shown in supplementary figure in (Fig.S6). We will combine the circuit and make custom made PCB in the future. A joystick controller for a user interface, **Fig. 3(a)** was integrated to wirelessly control Kraken up to 25ft. The program allows a user to select and activate each task, one at a time. The main menu selection starts by selecting between arms 1-4 or the buoyancy system. If an arm is chosen, the user can push up or down to actuate it to either grab or release an object. If the buoyancy system is chosen, the user can inflate or deflate the air bladder to control the vertical depth of Kraken. The overall sealing process is one of the most important processes for the underwater robot. We used Flex Seal Paint™, Flex Seal Tape™ and silicone EcoFlex 00-35 to seal the casing of Kraken (**Fig.2(c)**)

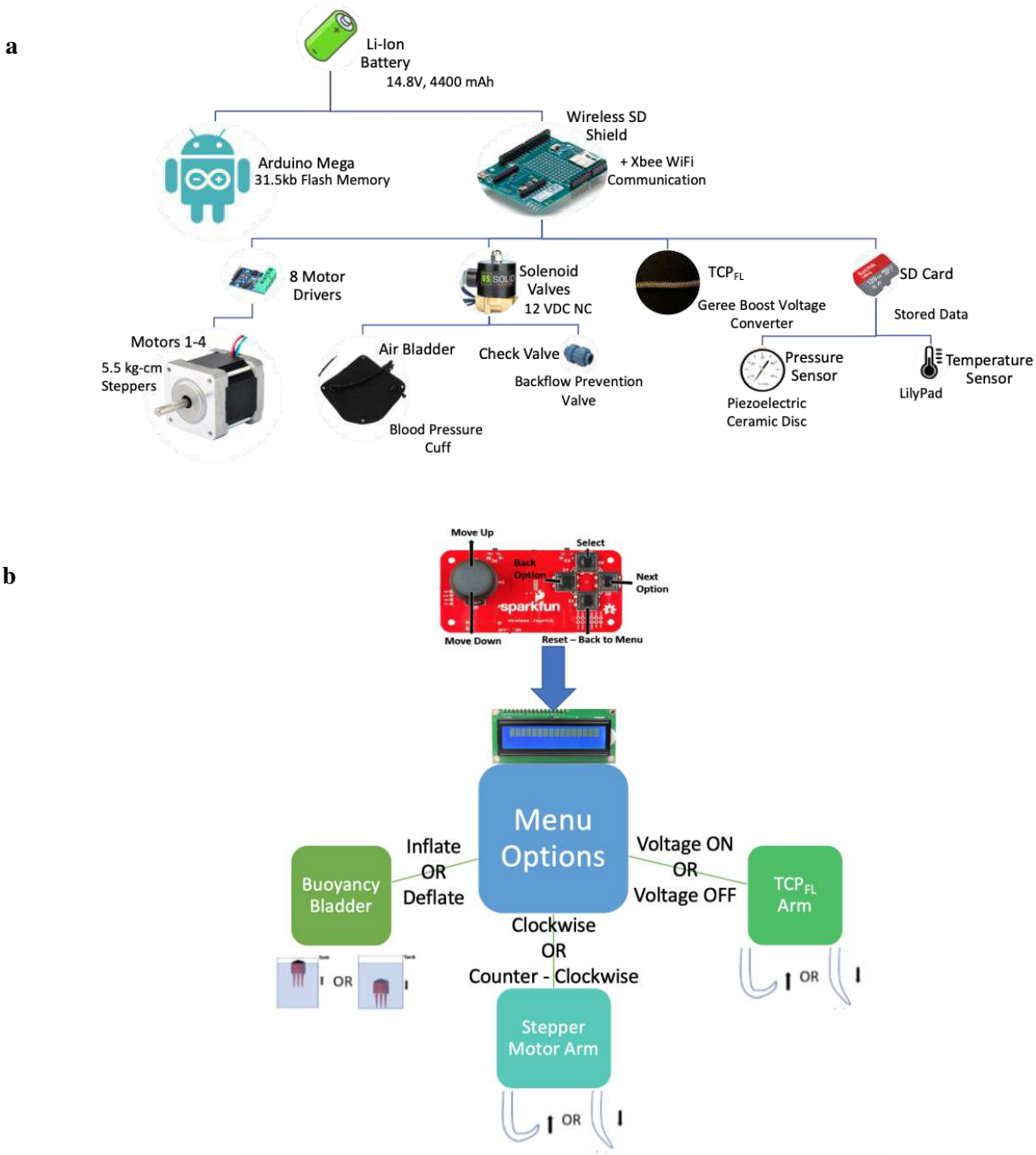

Fig. 3: (a) Wiring component diagram with snapshot of the wireless controlling joystick, (b) Programed controlling menu command.

2.6. Flow Simulation Process

An underwater flow simulation study of the vertical motion of our robot (the main body) is studied using ANSYS Fluent (v17.0) software and the analysis is a transient incompressible flow analysis. Yue et. al [44] suggests simplifying the 3D model to reduce the computational time and get more effective results for this type of underwater study. In our case, the model is split vertically in half in order to dimensionally reduce the domain. The mid-plane is assigned the symmetry boundary conditions while the sides of the domain are assigned as walls. The pressure is assumed constant throughout the domain because of the relatively small difference in vertical height. In order to impart the motion, a user-defined function is compiled in Fluent. The user-defined function consists of the physical properties of the robot. The surface of Kraken is assigned the fixed wall boundary condition $U\text{-}U_{wall} = 0$.

Two flow simulations were done. First, moving the model vertically upwards with a velocity of 1 m/s for 1s, giving it a Reynolds' number of around 5.7e5. Second, letting the robot sink under an acceleration of 0.0198 m/s^2 for 8s, which is calculated from the experiment (time-dependent velocity). Two methods can be used to define the interaction between the model and the fluid: (a) dynamic meshing, which sets the fluid as stationary and the model to move, and (b) fluid moving in the opposite direction as the model, which mimics the relative motion between the two [44]. Both these methods were analyzed by Leong et al. [45], who concluded that the results provided by both of them are just marginally different from the experimental results. A detailed description of the ANSYS Fluent simulation procedure and parameters are documented in the supplementary file (**Fig.S7**).

3. Results and Discussion

The summary of the test results is described quantitatively and qualitatively in this section. First, we will discuss the silicone arm configurations that provide various movements. This will be followed by the isotonic test results of the artificial muscle TCP_{FL}, and the embedded TCP_{FL} in the arm that was tested in a fish tank. Next, the underwater test results of the robot in a swimming pool using the stepper motors is discussed. Finally, the flow simulation results of the robot are presented.

3.1. Silicone arm configuration

One of the important parts of the robot is the flexible arm that is used for grasping different objects. Six different stiffness configurations are presented in **Fig.4(a-f)**. The variable arm stiffnesses are achieved by embedding different shapes and layouts of the spring steels, thickness of 0.003in (76µm), in the silicone as seen in **Fig.4(g)** during molding**. Fabrication steps are presented in the materials and methods section 2.4 and Fig.2(a).** The layout parameters, shown in **Fig.4(h)**, include changing the number of spring steels embedded (n), length (L), and thickness (t). The 2D bending on the XY plane is achieved as shown in **Fig.4(c and e),** while the 3D curling is achieved as shown in **Fig.4(a, b, d, and f).** Kraken's arms can be easily interchangeable by sliding them into the 3D printed arm lip and fastening using a hose clamp as shown in **Fig.4(i)**. The variability of the arm stiffness is dependent on the object it is aiming to grab. The different geometry and topology of the soft silicone and the very thin spring steel enable the arms to actuate in different modes. Each arm mounted in the robot (shown in **Fig.4(i)**) is different, making the robot unique and capable of handling different tasks. Different configurations are shown in movie 4. All the arms can be made with the same stiffness materials but that will limit the capability of the robot handling different objects. One basic scientific question we tried to answer in this case is how the actuation of the arm is influenced when the geometry and the materials are varied. Here, we showed that in order to have curling or bending actuations, like that of the natural octopus, it is not necessary to have a similar muscular hydrostat with so many radial and longitudinal muscles, instead, one actuator, namely a very thin, 76µm spring steel and 3mm silicone elastomer is enough for the arms to exhibit different motions that are essential for grasping objects. The six different arm configurations allow for a wide range of arm flexibility that can help divers and researches in underwater tasks such as holding equipment, samples, and interacting with live species delicately. We selected 4 arms to simplify the design of the robot. The addition of 4 more arms (to have a total of 8) will mimic the real octopus but will require a more complex electronic system and a bigger robotic structure. The use of 4 arms is also sufficient for grasping complex objects.

We have developed two different actuation systems to actuate the silicone arms. The first is utilizing a stepper motor as shown in Fig.5 (a). A tendon is embedded at the bottom of the silicone arm, and to maintain rigidity, fillers (cotton balls) are inserted in one of the arms (type VI). When the motor is turned ON, the arm is actuated as shown in the figure. On the other hand, the second actuation system is based on the TCP_{FL} as presented in Fig.5(b). Here, the TCP_{FL} is embedded at the bottom section of the arm. No fillers were added as the high actuation temperatures of the TCP_{FL} would burn the cotton balls. When the muscle is activated, the arm is actuated. Clearly, the difference between the two methods is on the number of structures and the magnitude of displacement provided by the artificial muscles and the motor rotation, which will determine the bending angles of the arms. The structure actuated by the stepper motor can bend and curl significantly as the motor can be rotate several rotations. But the TCP-actuated arm will have limited

bending angle as the maximum strain is 40% and the length of artificial muscle used is 110 mm long. There are pros and cons for each technology, and in fact this comparative analysis and study will be very helpful for considering various aspects such as weight and actuation issues. Performing theoretical analysis will help understand the structure better, but it requires a dedicated paper only focusing on the structure performance relationship of the composite deformable structures.

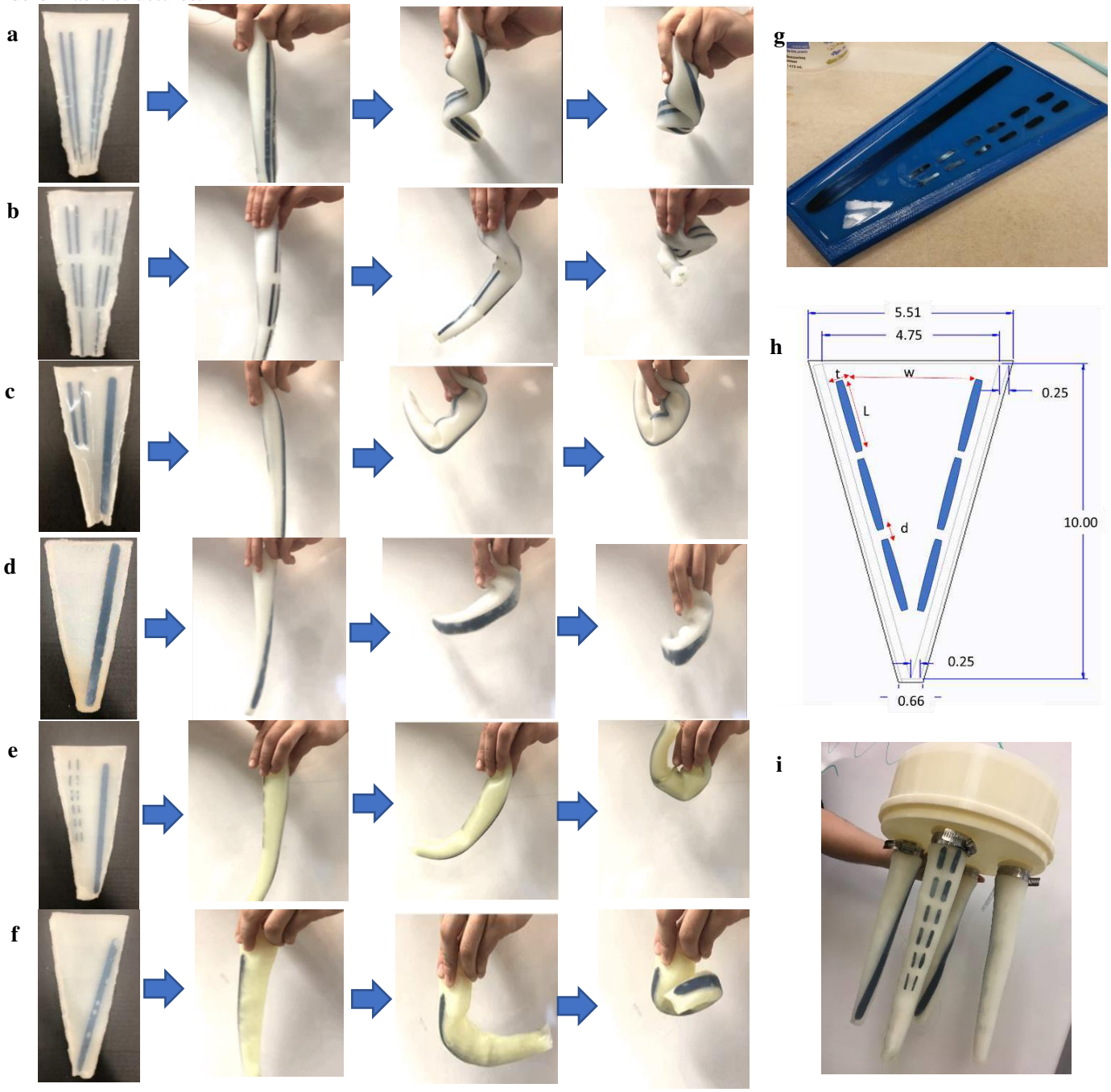

Fig. 4: **Different configuration of the octopus arm when spring steel, silicone and filler materials are changed: a** Double full length with no filler(Type I), **b** Sectioned double full length with no filler(Type II), **c** Half length on one side and full length on the other side with no filler added(Type III), **d** Full length added on one side with no filler(Type IV), **e** Sectional half-length on one side and single full length on the other side with no filler added(Type V), **f** Single full length added diagonally with filler(Type VI). **Molding method and assembly**: **g** Sample of spring steel embedded in silicone, **h** A schematics of octopus arm mold in (inches). In the figure, *t* is the thickness of the spring steel, *L* is the length, *d* is the distance, *n* is the number of spring steels embedded, **i** Different arm configurations (Type II, IV,V,VI) mounted on the robotic structure.

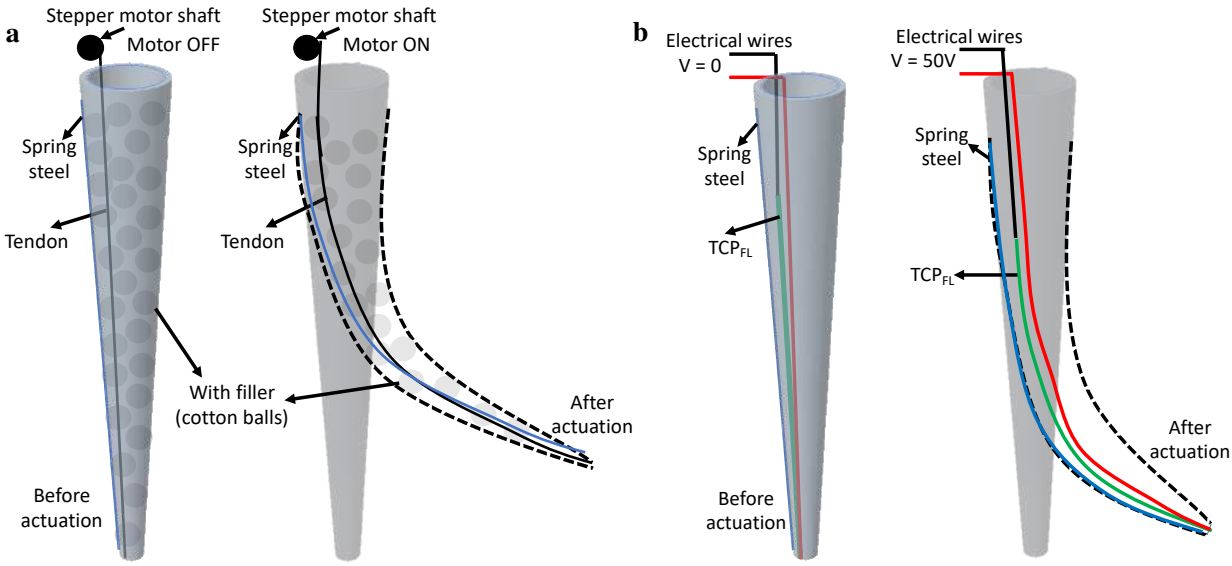

Fig. 5: Schematics of the actuation mechanisms: **a** utilizing stepper motors and **b** utilizing TCP_{FL}

3.2 TCP_{FL} isotonic testing

Testing of the novel actuator twisted and coiled polymer based on fishing line (TCP_{FL}) is essential to understanding its performance in various scenarios. The presented actuator is light in weight, flexible, inexpensive ($200/kg including nichrome); it can produce large strain and is capable of carrying weights up to 1000 times its own weight (TCP_{FL} 0.772g, can carry up to 800g, blocking load). These properties make this actuator suitable for many bioinspired swarm robots since we can make multiple robots without significant material cost. For example, if SMAs are used, they cost $3000/kg compared to the cost of TCPs.

There are limited studies available when it comes to TCP embedded in silicone elastomers such as studying the behavior of the TCP actuator's parameters and its overall performance in embedded condition.

Therefore, experiments are necessary for the TCPs, as well as when it is embedded within silicone.

To understand this, first, experimental characterization was performed on the self-coiled fishing line actuator (loaded length L=120 mm, diameter D = 2.8mm, resistance R = 312 Ω) without embedding in silicone. The photograph of the experimental setup and schematic diagram are shown in **Fig.6(a,b)**. The testing setup and experimental conditions are explained in detail in the *materials and methods* section and the supplementary document. A constant load of 300g was applied as a pre-stress parameter to the actuator because the maximum actuation stroke for fast actuation (2s ON and 50s OFF, 0.4A) is at this load. **Fig.6(c-e)** shows cyclic actuation strain, temperature, and power (2s ON and 50s OFF) for three electrical input current magnitudes. The actuator produces an amplitude strain of ~ 20% at 0.4A. **Fig.6(f-k)** show experimental results on the effect of input energy (heating time, voltage, and current) on the actuation performance (stroke %) and temperature change while still maintaining a constant cooling time of 50s**. Fig.6(f,g)** are results for 0.2A input current with the variation of heating time from 2s to 7s, where an increase of 13% in the actuation strain is observed**. Fig.6(h,i)** are for 0.3A input current and variation of the heating from 2s to 4s, which shows an increase of almost 20% actuation strain. Likewise, **Fig.6(j,k)** are for 0.4A current with heating times of 1s and 2s, an increase of 13% is also observed. The results show that increasing the input energy will significantly increase the performance of the actuator. The input energy is the product of power and heating time. An average of 20% strain is achieved at a temperature of 100^0C for all 3-current magnitudes with varying energy consumptions.

The variation of input current and heating time is very critical due to the temperature sensitivity of the actuator. If the temperature exceeds its melting point 250°C when heat is applied, the muscle will burn and will no longer actuate. Equation (1) can be used for the temperature prediction according to the electrical input.

$$T(t) = -\frac{R_o i^2}{-hA + R_o i^2 \alpha}\left(1 - e^{\frac{-hA+R_o i^2 \alpha}{mc_p}t}\right) + T_\infty \qquad (1)$$

where $T(t)$ is the temperature of the actuator at time t, T_∞ is the ambient room temperature, R_o is the resistance of the actuator at room temperature, i is the input current, A is the cross-sectional area of the precursor fiber of the actuator (nylon), m is the mass of the actuator, c_p is specific heat, and α is the temperature coefficient for the resistivity.

The resistance change of the muscle is due to the temperature change [46], which is calculated using Equation (2).

$$R(t) = R_0[1 + \alpha(T(t) - T_\infty)] \quad (2)$$

The temperature coefficient of resistance of the nichrome wire is α = 5.78 x 10^{-4}/°C [47] and the ambient temperature T_∞ = ~23°C. We can predict the resistance change during actuation with respect to time.
Equation (3) and (4) can be used to calculate the electrical power (P) and electrical energy (E) provided to the actuator, by adjusting the electrical current input (I), input voltage (V) and duration of input time (t).

$$P = I\,V \quad (3)$$
$$E = Pt = I\,Vt \quad (4)$$

By observing the actuation results for the TCP_{FL} from **Fig.6 (c, d, and e)**, we can see that the actuation stroke is dependent on the input current (Δ=0.1A difference) and the time the current is applied (an order of 1s to 7s). Equation (3) and (4) can be used to calculate the energy consumed which is shown to affect the TCP_{FL} performance. We noted earlier that in all three cases in **Fig.6.(g-l)** almost a 13% strain increase is achieved at higher energy values. Considering, **Fig.6 (e)** (input power at different current magnitudes), and **Fig.6 (f)** (The actuation strain at 0.2 A, for 2 s and 7s), the input energy is E = 15Wx 2s = 30 J for the 2 second heating. Similarly, for 7 seconds heating, E = 15W x 7s = 105 J. Therefore, we can say that the increase of energy from 30J to 105 J results in the 13% actuation strain increase. Similar properties are observed for the other plots for **Fig.6 (h and i).** The cooling cycle also affects the displacement of the actuator, which is visible in the cooling cycles, showing exponential decay. A bias is observed in the actuation strain at 50s (when the first cycle is finished), which is an indication that higher cooling times are needed to decrease the bias. In our robotic application, an increase in the heating time is needed to help the arm achieve higher bending angles and to tightly curl the arm after running for a few cycles. However, this will result in low frequency. Some of the drawbacks of this actuator are the low frequency (below 7 Hz [1]) and low efficiency (below 1%), but the contractile efficiency per weight of the actuator is 12.64%/kg. The efficiency is the ratio of the energy output to the electrical input energy. There are some solutions to improve the performance in energy efficiency and actuation such as pulsed actuation [4], active cooling [48,49], and a locking mechanism [50].

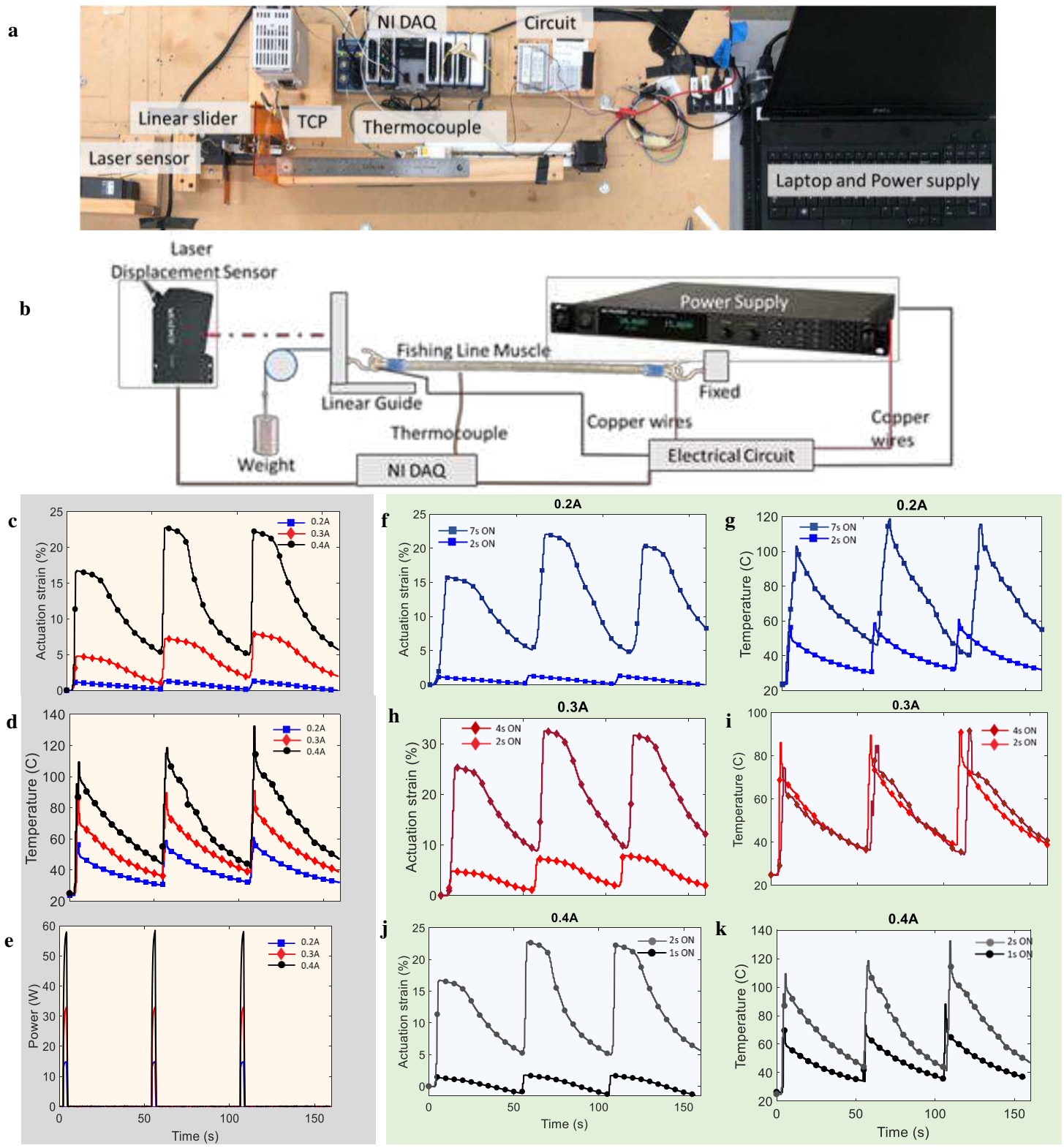

Fig. 6: Experimental characterization of self-coiled with nichrome TCP$_{FL}$ actuator: a Isotonic test experimental set up, **b** Experimental schematics. Three cycles experimental results at 2s ON and 50s OFF for 0.2A,0.3A, and 0.4A input current: **c** Actuation strain, **d** Temperature, **e** Power, **f&g** Effect of heating time on actuation strain and temperature for 0.2A, **h&i** for 0.3A, **j&k** for and 0.4A. Markers are skipped at an increment of 50 data points.

3.3 TCP_{FL} embedded in the arm and tested in a fish tank

The second set of experiments was the actuator in embedded conditions. We present the TCP_{FL} actuator with a length of 100 mm (R = 335 Ω, pre-stress at 300g loading) embedded in one of the silicone arms and tested in both air and underwater using a 70-gallon fish tank in a lab setting (the test in the air was at room temperature, the water temperature was 21°C). The experimental set up is shown in the schematics in **Fig.S3(a,b)**. **Fig.7(a and b)** show the schematic diagram and photograph of the actuator embedded in the arm showing the bending angle. The silicone arm triggered by the TCP_{FL} actuator shows good potential for grasping due to its high bending angle. **Fig.7(c)** shows the effect of input current on the bending angle for the actuation in air medium and in underwater conditions respectively. When tested in air, an increase in current increases the bending actuation in a non-linear fashion except a slight decrease when the current is 0.2A for all heating time (10, 15 and 20 s). This could be due to the heat trapped within the silicone, which prevents further actuation. In water, the trend is slightly different. Overall, the increase in energy results in an increase in bending. **Fig.7(c)** shows that the bending angle in air and in underwater is almost doubled when the energy is doubled. For example, at 0.2A with 10s and 20s heating the power consumption is ~13W ($P = R*I^2$, assuming constant resistance) the energy would be 130J and 260J respectively which results in an increase of bending angle from 10° to 20°. **Fig.7(d)** shows results for the bending angle vs. time for both in air and underwater conditions. In the air, the arm can bend up to a maximum of 38° from its original position at an input current of 0.16A for 20s heating (output voltage is 54V). In the water, it can bend up to 21° using the same energy consumption. **Fig.6(e)** presents cyclic actuation results in underwater conditions. Here, it is also observed that the higher bending angles are produced at higher energy values with continuous heating. Movie 5 and movie 6 show the arm actuating in underwater conditions.

After implementing the actuator in the silicone arm (configuration 5, **Fig.4(f)**) at pre-stress of 3N, the test results showed that the arm could achieve a maximum of the 40° bending angle in air medium (**Fig.7 (d)**), compared to the 21° angle in underwater conditions at the same input current and heating time. The decrease in the bending angle in underwater medium is due to several factors. First, the cold temperature of the water prevented the actuator from reaching its optimal temperature for maximum bending, which is why increasing the heating time was necessary during experiments. This is related to the convective and conductive heat transfer process, which needs further study via modeling and simulation. Second, while actuating in air medium, the arm is faced with minimal external forces. But, while actuating in underwater conditions, the arm is subjected to external forces (distributed pressure load) such as the pressure due to depth and damping force. Multiple actuators can be added in parallel in each arm in order to enhance the grasping performance of the silicone arms. Moreover, a locking mechanism [50] can be implemented to achieve tasks such as grabbing and holding. These would be beneficial for applications related to underwater data sampling. **Fig.7(f-h)** presents the TCP_{FL} arm lifting representative objects that are anchored using a string at the tip. The arm can lift objects such as PVC pipe and calibrated weights. Movie 7 shows the fishing line arm capable of lifting objects underwater. Due to the large voltage required to actuate the TCP_{FL} actuators, in order to wirelessly control the actuator using a battery, a step-up voltage converter was added to the controlling circuit as shown in **Fig.S7 (a).** This circuit is capable of increasing the voltage from 14.8V up to 130V which is more than sufficient to provide the voltage needed to use the TCP_{FL} at its maximum performance.

3.4 Testing underwater in a swimming pool using the stepper motors

The third set of experiments was a field test of the robot to show the robustness of the design. Kraken is completely functional when submerged underwater, as shown in supplementary movie1, **Fig.7,** and **Fig.S4**. Testing in the swimming pool was conducted using the stepper motors powered by an onboard Li-ion battery as the primary source of arm actuation. Grasping of a small PVC pipe can be observed in **Fig.7(i, j, and k)** and movie 2. A 2.5 kg weight is attached to the robot as shown in **Fig.7(l)**. Kraken is still able to float while carrying heavy loads as shown in **Fig.7(m)**. **Fig.7(n)** shows a snapshot of the octopus floating on the surface with silicone arms fully extended. **Fig.7(o)** shows an interesting configuration of 3 arms actuated at their different curling motions using the mode shown earlier in **Fig.7(c, d, and f)**. The ability to bend its arms according to the situation while maintaining a minimum size or profile is one unique feature of this robot. Moreover, vertical swimming while carrying a heavy load is presented. **Fig.7(p)** shows Kraken releasing air to sink to the bottom surface of the pool, also shown in the supplementary movie 3. Lastly, **Fig.7(q)** shows Kraken carrying both the heavy payload and grasping the PVC pipe.

Kraken has a lot of potential in assisting underwater research and works, such as replacing remotely operated vehicles and underwater explorations, pipe opening/closing and cleanups. It can also save lives in a swimming pool or the ocean when a camera is mounted in the body using artificial intelligence, when it is fully developed. The stress simulation results in **Fig.S9** in the supplementary show that the cage with carbon fiber material would be structurally safe to operate at depths up to 100 ft under stress of 60 MPa (3.02 atm pressure).

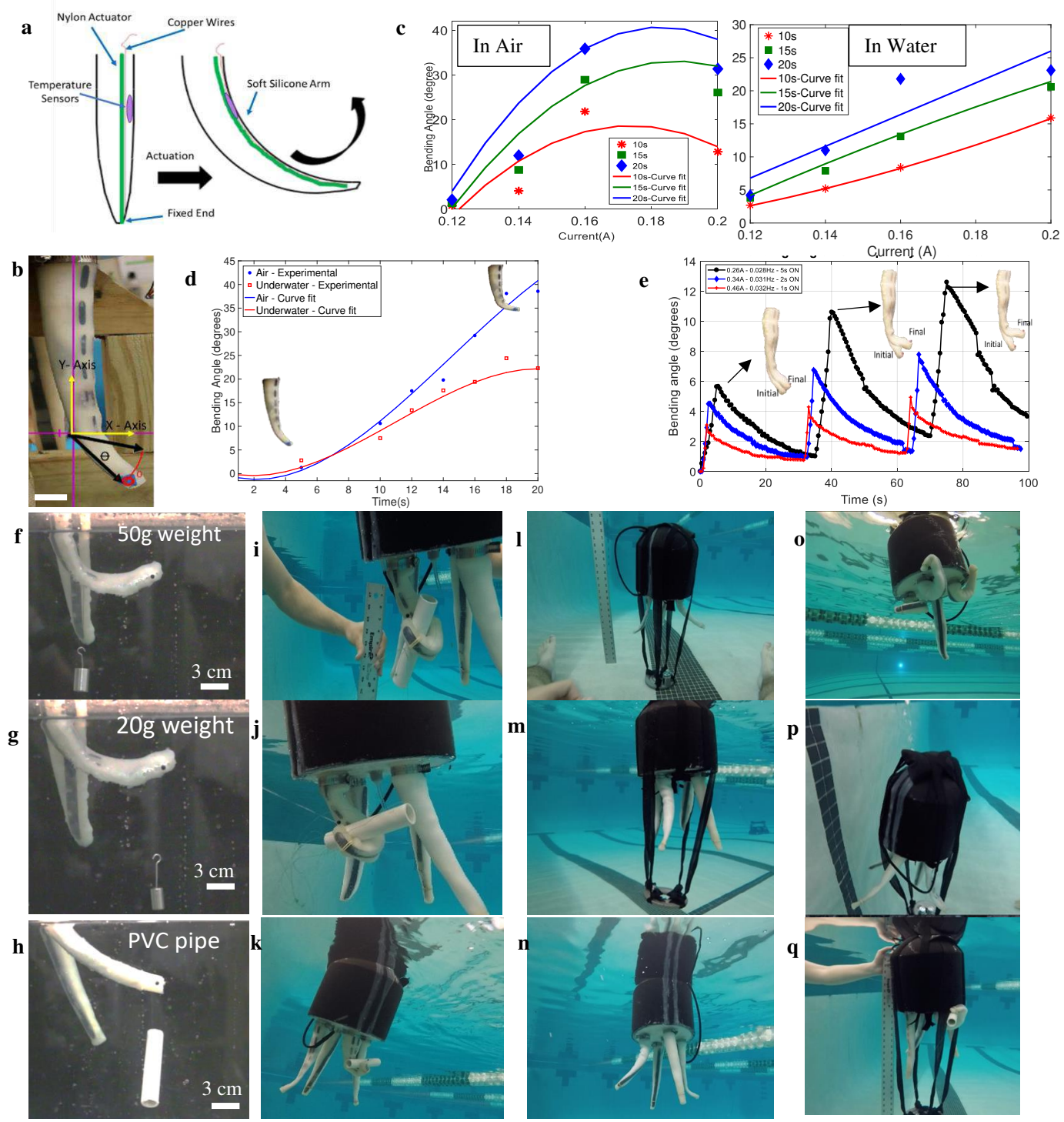

Fig. 7: Charactrization of the Kraken arms.: a Schematics of the muscle connections (TCP_{FL} length = 100mm), b TCP octopus arm showing bending angle**, c** Bending angle vs input current at different time points (left in air and right in the water), **d** Bending angle vs time at input current of 0.16A in air and in underwater condition. Tested in air and in underwater conditions, **e** Cyclic underwater actuation for low, medium, and high input current with variation of duty cycles**. Experimental TCP_{FL} silicone arm grasping objects in a 70-gallon fish tank: f-g** 50g and 20g calibrated weight hanging on a wire, **h** Small PVC hooked on a wire. **Kraken deployed in a swimming pool (depth 6ft) actuated by stepper motors: i,j,k** Grapsing of PVC pipe, **l,m,n** Arms in resting position while carrying 2.5kg payload, **o** Curling of octopus arms, **p** Bouyancy system releasing air, robot sinking, **q** Floating while grasping PVC with 2.5kg payload

3.5 Flow Simulation Results

To understand the fluid-structure relationship while the robot is moving, flow studies are performed, keeping the solid model of the robot. The simulation set up is explained in the previous section in 2.6 *"flow simulation process"* in the main text and more information in the supplementary material. Essentially, the fluid domain (surrounding environment) and rigid body (Kraken's body) are defined, the rigid body (Kraken) was subjected to have a velocity, and the pressure at the top and bottom were set to be zero. The simulation was performed in ANSYS. The results show that the flow is only affected in the close vicinity of the rigid body motion of Kraken but the magnitude and pattern of curling, circulation and other properties are essential to understand the behavior. **Fig.8 (a-d)** shows the simulation results of Kraken's rigid body motion moving upwards while **Fig.8 (e-h)** shows the results of Kraken's movement sinking downwards. In the first set of figures (**Fig.8(a-d)**) it is shown that the streamlines propagates from Kraken in the opposite direction of the movement, leaving behind turbulent recirculation (shown in the bottom corner in the left and right of the rigid body) similar to what is expected from an underwater rigid body motion. This upward motion simulation is implemented at a much higher speed (1 m/s) and hence causing the generation of more circulations.
This can also be accounted for the fact that the wake surface has a sharp edge while rising, whereas the wake surface has a smoother surface transition while sinking. These results will be useful to determine the flow behavior of UUVs (unmanned underwater vehicles). The sinking acceleration is very small (~0.02 m/s^2, measured from experiments) due to buoyancy and viscous drag acting on the body. The wall shear (τ_{ij}) is calculated by equation (5) and the results are shown in **Fig.8 (i-k)** with the corresponding legend in the left side.

$$\tau_{ij} = \mu_i u_j + \mu_j u_i \tag{5}$$

μ_i and $\mu_j$are the dynamic viscosity in the x and y direction, and u_j and u_i instantaneous velocities in the y and x directions. The flow field resulting from the motion of Kraken is calculated by the unsteady incompressible Reynolds-averaged Navier Stokes (RANS) equations as shown in equation 6 and 7:

$$\frac{\partial u_j}{\partial x_j} = 0 \tag{6}$$

$$\frac{\partial u_i}{\partial t} + \frac{\partial u_i u_j}{\partial x_j} = -\frac{1}{\rho}\frac{\partial P}{\partial x_i} + \nu \frac{\partial}{\partial x_j}\left[\left(\frac{\partial u_i}{\partial x_j} + \frac{\partial u_j}{\partial x_i}\right)\right] - \frac{\partial \overline{u_i' u_j'}}{\partial x_j} \tag{7}$$

where u_i and u_i' are the mean and fluctuating components of the instantaneous velocity, P is the mean component of instantaneous pressure and ν is the kinematic viscosity. The realizable k- ε turbulence model with scalable wall functions solver is used to study the dynamics of the fluid domain.

The flow simulation model presented in **Fig.8** can help in studying different designs of Kraken computationally, which can save time and resources spent on experimental studies. These design iterations can include different structure designs based on different geometries of the outside sealing structure housing of Kraken, mass of the rigid body, different surrounding fluids (fresh water, ocean water etc.) at various depths in which Kraken is deployed, and lastly, different surrounding temperatures. The presented turbulent model can provide accurate and superior performance in the flows involving recirculation [51]. The surrounding pressure (contour plot shown in the right side) is not affected much with time since the speed gained by the body is very small to cause considerable flow separation as shown in **Fig.8 (i-k).** The velocity contour is consistent with the one shown by Yue et al. [45], the only difference being that Yue et al. [45] has a stationary body and moving fluid, while our model has stationary fluid and moving body. The wall shear contour obtained corresponds to the profiles shown by Wang et al. [52], Zhang et al. [53], and Zhou et al. [54] for their respective underwater simulations. Fig.8 (l-n) shows the simulation parameters used in the study. More studies can be done on the recirculation generated if they can be helpful for other things such as energy harvesting. This new robot has the capability of opening new doors in underwater exploration and can lead to new discoveries and understanding the world beneath our waters.

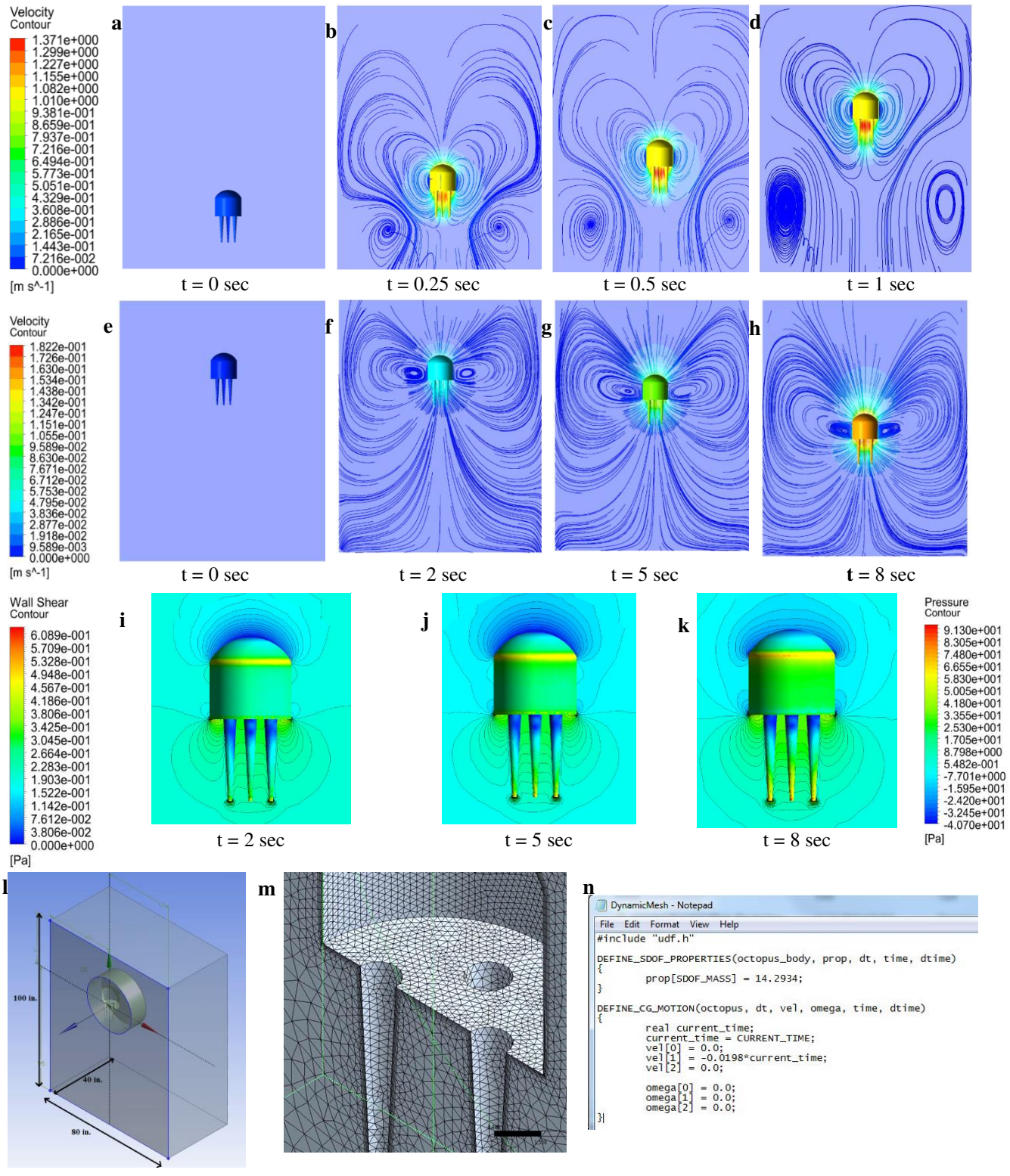

Fig. 8: Flow simulation for Kraken: a-d Flow field generated around the Kraken moving up with constant speed of 1m/s at various times**, e-h** Flow field generated around the Kraken accelerating downwards at 0.0198 m/s^2 at various times, **i-k** Pressure contours around and wall shear on surface of Kraken accelerating downwards at various times. **l-n** Simulation set up and mesh parameters in ansys fluid simulation

4 Conclusion and Future Work

In this paper, we presented a novel octopus-like robot known as Kraken that is actuated by a hybrid system consisting of stepper motors and an artificial muscle. The robot has four different flexible tentacles that allow grasping of objects in different modalities. We showed experimental results of the robot deployed in a swimming pool as shown in **Fig.1 (b, c, e, f)** and in movie 8. A summary of important features of the robot is presented in table 1 and compared with others. There have been some octopus-like robots shown in the literature that have gripper arms but do not swim, others that are only capable of swimming, and others that are capable of both swimming and grasping. Significant data and experimental results have been generated from other research groups, which helped the current study. Unlike what we presented, most of the robots in the literature lack one or more feature such as the variability of arm stiffness or multimodal bending. Most of them do not include an onboard buoyancy system, powering means or untethered operation. The inexpensive novel actuators integrated into the Kraken robot offer an actuation stroke up to 40% at 3N load, which is a unique feature of our robot. The TCP_{FL} actuators were extensively characterized experimentally to understand the behavior (**Fig.6 & Fig.7**), and we showed excellent bending of the robot's arm. The actuator is significantly smaller and lighter than the stepper motors allowing for further advancement in reducing the size and shape of the robot that is inspired by nature. The hybrid system was tested in both a lab setting (TCP arm, movie 5, 6, 7) and in a swimming pool (stepper motor arms, movies 1, 2, 3, 8). To study the fluid structure relationships and flow behavior of the robot simulations were carried out and analyzed.

The highlights of Kraken robot are as follows:

- Kraken utilizes a combined actuation system of both stepper motors and an artificial TCP_{FL} actuator.
- Kraken is wirelessly controlled through a communication between the onboard controlling circuit and the wireless joystick that can be located at distances up to 25ft.
- The robot can operate for 45 minutes using the onboard lithium ion battery.
- Kraken's buoyancy system allows it to swim vertically at various depths.
- Kraken is presented with different arm configurations in **Fig.2** (movie 4) that can produce variable bending and curling capabilities of the arm tailored to grasp various objects underwater.

Future work will include developing a custom-made controlling circuit, analytical modeling and control algorithms. Optimized mechanical design of the robot includes material choice and structural arrangement. Moreover, the implementation of a high performance inertia measurement unit (IMU) for sensing and balancing the system underwater. Further testing should be done using other types of silicone elastomers, stiffness control, and actuation parameters to determine an optimized octopi's structure for oceanic exploration. When developed further, it would be feasible for the TCP_{FL} actuators to replace the stepper motors and increase space for other sensory equipment such as cameras, chemical sensors, seismographs, or other equipment useful in exploration that would previously require a much larger robot.

Due to the size of the robot as well as the minimal impact it makes in terms of noise and vibrations of the TCP_{FL} actuator, the robot can serve as an exploratory tool in situations where minimal interference is necessary. Typical mission-specific scenarios may require a delicate touch where noise and vibrations would alert other life. We observed that the stepper motors have some noise during underwater testing, which should not be ignored. Meanwhile, the flexibility of the arms, when developed further, will allow the robot to grasp objects when space is limited. This will lead to a higher adaptability when dealing with situations where space will be an issue, such as crevices. We hope that the results presented can be a stepping-stone in improving underwater robots and can be relevant to other researchers who would like to mimic the structure. It should be noted that we did not attempt to mimic the entire structure of an octopus arm that has complex muscle arrangements, suction cups, and a deformable body structure (the mantle), we only took a few of the important structures and demonstrated a fully functional field robot that can assist human being in different scenarios as shown in movie 8.

Acknowledgments

The authors would like to thank Davis Fletcher, Anthony Reyes, Hieu Doan, Norman Peters for their great contribution to the design and development of the robot in their senior design project. Armita Hamidi and Jeremy Warren for their comments and discussion. We would like to dedicate this study in the loving memory of Hieu Doan (1997-2019).

Funding: The authors would like to acknowledge the support of the Office of Naval Research (ONR), Young Investigator Program, under Grant No. N00014-15-1-2503.

Authors contributions: Y.A., M.S., M.P., designed the robot. Y.A. contributed to experimental results and analysis of the TCP actuator and arm actuation. M.S., M.P conducted the swimming pool experimental test. S.S contributed to the modeling and computational fluid analysis. Y.T. conceived the idea of the robot, bioinspiration and led the project**.** All authors conceived the experimental work, wrote the paper, and provided feedback.

Competing interest: The authors declare they have no competing interests.

Supplementary Material

Fig. S1: Examples of presented octopus like robot found in the literature.
Fig. S2: Fabrication of fishing line muscle with thin heating wire
Fig. S3: Muscle characterization isotonic test set up
Fig. S4: Connectivity diagram of the robot's components.
Fig. S5: Steps of molding the silicone arm, assembling robot, and water sealing.
Fig. S6: Schematics of robot's controlling circuit.
Fig. S7: Computational domain of interest for the flow simulation, meshed model, and a snippet of the user-defined function (UDF) used for assigning the motion of the model.
Fig. S8: Experimental set up for TCP actuated arm (underwater and in air).
Fig. S9: Finite element analysis for 3D printed structure due to change of surrounding pressure.

Movie 1	Kraken, octopus like robot deployed for underwater testing in an Olympic size swimming pool. https://youtu.be/Hjv_z-EOwW8
Movie 2	Kraken, octopus robot fully functioning in a swimming pool. Grasping objects utilizing stepper motor hybrid actuation system. https://youtu.be/Tf8EwqJO1Vw
Movie 3	Kraken, octopus robot buoyancy system test for vertical swimming in a swimming pool (sinking and floating) https://youtu.be/UAuI5uTm59A
Movie 4	Kraken's designed six soft silicone arms showing the effect of stiffness on grasping modalities. https://youtu.be/g9l0Orj4ojo
Movie 5	Under water cyclic actuation at 0.032Hz frequency (input current of 0.26A with 5s heating) of the self-coiled twisted and coiled polymer fishing line actuator embedded silicone octopus arm. https://youtu.be/pEfsrprXY7Y
Movie 6	Underwater actuation of the self-coiled fishing line actuator arm at various input currents (0.12A-0.2A) https://youtu.be/1bI2ZaZf28w
Movie 7	Underwater grasping of objects such as a PVC pipe, 8.4oz filled can, and calibrated weight using the self-coiled fishing line actuator arm https://youtu.be/gyat05d1lPE
Movie 8	Kraken octopus robot deployed in the swimming pool displaying multiple functionalities such as grasping and releasing and curling of multiple arms, highlighting the safe human interaction aspect of this robot. https://youtu.be/z2dfYvrlkaE
Movie 9	Fabrication process of self-coiled fishing line actuator. https://youtu.be/LtMKnp6tuhM

References

1. Haines, C.S., Lima, M.D., Li, N., Spinks, G.M., Foroughi, J., Madden, J.D., Kim, S.H., Fang, S., De Andrade, M.J., Göktepe, F.: Artificial muscles from fishing line and sewing thread. science **343**(6173), 868-872 (2014).
2. Almubarak, Y., Tadesse, Y.: Twisted and coiled polymer (TCP) muscles embedded in silicone elastomer for use in soft robot. International Journal of Intelligent Robotics and Applications **1**(3), 352-368 (2017).
3. Saharan, L., Andrade, M.J.d., Saleem, W., Baughman, R.H., Tadesse, Y.: iGrab: Hand Orthosis Powered by Twisted and Coiled Polymer Muscles. Smart Materials and Structures (2017).
4. Wu, L., de Andrade, M.J., Saharan, L.K., Rome, R.S., Baughman, R.H., Tadesse, Y.: Compact and low-cost humanoid hand powered by nylon artificial muscles. Bioinspiration & biomimetics **12**(2), 026004 (2017).
5. Hamidi, A., Almubarak, Y., Rupawat, Y.M., Warren, J., Tadesse, Y.: Poly-Saora robotic jellyfish: swimming underwater by twisted and coiled polymer actuators. Smart Materials and Structures **29**(4), 045039 (2020).
6. Hamidi, A., Almubarak, Y., Tadesse, Y.: Multidirectional 3D-printed functionally graded modular joint actuated by TCP FL muscles for soft robots. Bio-Design and Manufacturing **2**(4), 256-268 (2019).
7. Wu, L., Chauhan, I., Tadesse, Y.: A novel soft actuator for the musculoskeletal system. Advanced Materials Technologies **3**(5), 1700359 (2018).
8. Almubarak, Y., Punnoose, M., Maly, N.X., Hamidi, A., Tadesse, Y.: KryptoJelly: A jellyfish robot with confined, adjustable pre-stress, and easily replaceable shape memory alloy NiTi actuators. Smart Materials and Structures (2020).
9. Morimoto, Y., Onoe, H., Takeuchi, S.: Biohybrid robot powered by an antagonistic pair of skeletal muscle tissues. Science Robotics **3**(18), eaat4440 (2018).
10. Nawroth, J.C., Lee, H., Feinberg, A.W., Ripplinger, C.M., McCain, M.L., Grosberg, A., Dabiri, J.O., Parker, K.K.: A tissue-engineered jellyfish with biomimetic propulsion. Nature biotechnology **30**(8), 792 (2012).
11. Mintchev, S., Shintake, J., Floreano, D.: Bioinspired dual-stiffness origami. Science Robotics **3**(20), eaau0275 (2018).
12. Tomar, A., Tadesse, Y.: Multi-layer robot skin with embedded sensors and muscles. In: Electroactive Polymer Actuators and Devices (EAPAD) 2016 2016, p. 979809. International Society for Optics and Photonics
13. Stiehl, W.D., Lalla, L., Breazeal, C.: A" somatic alphabet" approach to" sensitive skin". In: Robotics and Automation, 2004. Proceedings. ICRA'04. 2004 IEEE International Conference on 2004, pp. 2865-2870. IEEE
14. Sanford, J., Ranatunga, I., Popa, D.: Physical human-robot interaction with a mobile manipulator through pressure sensitive robot skin. In: Proceedings of the 6th International Conference on Pervasive Technologies Related to Assistive Environments 2013, p. 60. ACM
15. Katzschmann, R.K., DelPreto, J., MacCurdy, R., Rus, D.: Exploration of underwater life with an acoustically controlled soft robotic fish. (2018).
16. Coral, W., Rossi, C., Curet, O.M., Castro, D.: Design and assessment of a flexible fish robot actuated by shape memory alloys. Bioinspiration & biomimetics **13**(5), 056009 (2018).
17. Villanueva, A., Smith, C., Priya, S.: A biomimetic robotic jellyfish (Robojelly) actuated by shape memory alloy composite actuators. Bioinspiration & biomimetics **6**(3), 036004 (2011).
18. Frame, J., Lopez, N., Curet, O., Engeberg, E.D.: Thrust force characterization of free-swimming soft robotic jellyfish. Bioinspiration & biomimetics **13**(6), 064001 (2018).
19. Joshi, A., Kulkarni, A., Tadesse, Y.: FludoJelly: Experimental Study on Jellyfish-Like Soft Robot Enabled by Soft Pneumatic Composite (SPC). Robotics **8**(3), 56 (2019).
20. Mather, J.A.: How do octopuses use their arms? Journal of Comparative Psychology **112**(3), 306 (1998).
21. Kazakidi, A., Kuba, M., Botvinnik, A., Sfakiotakis, M., Gutnick, T., Hanassy, S., Levy, G., Ekaterinaris, J.A., Flash, T., Hochner, B.: Swimming patterns of the octopus vulgaris. In: 22nd Annual Meeting NCM Society 2012, pp. 23-29
22. Sfakiotakis, M., Kazakidi, A., Pateromichelakis, N., Tsakiris, D.P.: Octopus-inspired eight-arm robotic swimming by sculling movements. In: Robotics and Automation (ICRA), 2013 IEEE International Conference on 2013, pp. 5155-5161. IEEE
23. Sfakiotakis, M., Kazakidi, A., Tsakiris, D.: Octopus-inspired multi-arm robotic swimming. Bioinspiration & biomimetics **10**(3), 035005 (2015).
24. Mazzolai, B., Margheri, L., Laschi, C.: Quantitative measurements of Octopus vulgaris arms for bioinspired soft robotics. In: Metrics of Sensory Motor Coordination and Integration in Robots and Animals. pp. 3-14. Springer, (2020)

25. Arienti, A., Calisti, M., Giorgio-Serchi, F., Laschi, C.: PoseiDRONE: design of a soft-bodied ROV with crawling, swimming and manipulation ability. In: Oceans-San Diego, 2013 2013, pp. 1-7. IEEE
26. Serchi, F.G., Arienti, A., Laschi, C.: Biomimetic vortex propulsion: toward the new paradigm of soft unmanned underwater vehicles. IEEE/ASME Transactions On Mechatronics **18**(2), 484-493 (2013).
27. Festo: OctopusGripper and BionicCobot (undated). https://www.festo.com/group/en/cms/12745.htm
28. Fras, J., Noh, Y., Macias, M., Wurdemann, H., Althoefer, K.: Bio-inspired octopus robot based on novel soft fluidic actuator. In: 2018 IEEE International Conference on Robotics and Automation (ICRA) 2018, pp. 1583-1588. IEEE
29. Calisti, M., Giorelli, M., Levy, G., Mazzolai, B., Hochner, B., Laschi, C., Dario, P.: An octopus-bioinspired solution to movement and manipulation for soft robots. Bioinspiration & biomimetics **6**(3), 036002 (2011).
30. Sfakiotakis, M., Kazakidi, A., Tsakiris, D.P.: Turning maneuvers of an octopus-inspired multi-arm robotic swimmer. In: Control & Automation (MED), 2013 21st Mediterranean Conference on 2013, pp. 1343-1349. IEEE
31. Sfakiotakis, M., Kazakidi, A., Chatzidaki, A., Evdaimon, T., Tsakiris, D.P.: Multi-arm robotic swimming with octopus-inspired compliant web. In: Intelligent Robots and Systems (IROS 2014), 2014 IEEE/RSJ International Conference on 2014, pp. 302-308. IEEE
32. Laschi, C., Cianchetti, M., Mazzolai, B., Margheri, L., Follador, M., Dario, P.: Soft robot arm inspired by the octopus. Advanced Robotics **26**(7), 709-727 (2012).
33. Mazzolai, B., Margheri, L., Cianchetti, M., Dario, P., Laschi, C.: Soft-robotic arm inspired by the octopus: II. From artificial requirements to innovative technological solutions. Bioinspiration & biomimetics **7**(2), 025005 (2012).
34. Cianchetti, M., Calisti, M., Margheri, L., Kuba, M., Laschi, C.: Bioinspired locomotion and grasping in water: the soft eight-arm OCTOPUS robot. Bioinspiration & biomimetics **10**(3), 035003 (2015).
35. Ito, K., Homma, Y., Rossiter, J.: The soft multi-legged robot inspired by octopus: climbing various columnar objects. Advanced Robotics, 1-14 (2020).
36. Jiao, J., Liu, S., Deng, H., Lai, Y., Li, F., Mei, T., Huang, H.: Design and Fabrication of Long Soft-Robotic Elastomeric Actuator Inspired by Octopus Arm. In: 2019 IEEE International Conference on Robotics and Biomimetics (ROBIO) 2019, pp. 2826-2832. IEEE
37. Dai, Y., Chen, D., Liang, S., Song, L., Qi, Q., Feng, L.: A Magnetically Actuated Octopus-like Robot Capable of Moving in 3D Space. In: 2019 IEEE International Conference on Robotics and Biomimetics (ROBIO) 2019, pp. 2201-2206. IEEE
38. Thuruthel, T.G., Falotico, E., Renda, F., Flash, T., Laschi, C.: Emergence of behavior through morphology: a case study on an octopus inspired manipulator. Bioinspiration & Biomimetics **14**(3), 034001 (2019).
39. Kwak, B., Bae, J.: Locomotion of arthropods in aquatic environment and their applications in robotics. Bioinspiration & biomimetics **13**(4), 041002 (2018).
40. Salazar, R., Campos, A., Fuentes, V., Abdelkefi, A.: A review on the modeling, materials, and actuators of aquatic unmanned vehicles. Ocean Engineering **172**, 257-285 (2019).
41. Salazar, R., Fuentes, V., Abdelkefi, A.: Classification of biological and bioinspired aquatic systems: A review. Ocean Engineering **148**, 75-114 (2018).
42. Edwards, P., Pálsson, H.: Arrow-Odd: a medieval novel. New York University Press New York, (1970)
43. Semochkin, A.N.: A device for producing artificial muscles from nylon fishing line with a heater wire. In: Assembly and Manufacturing (ISAM), 2016 IEEE International Symposium on 2016, pp. 26-30. IEEE
44. Yue, C., Guo, S., Li, M.: ANSYS FLUENT-based modeling and hydrodynamic analysis for a spherical underwater robot. In: Mechatronics and Automation (ICMA), 2013 IEEE International Conference on 2013, pp. 1577-1581. IEEE
45. Leong, Z.Q., Ranmuthugala, D., Penesis, I., Nguyen, H.D.: Computational fluid dynamics re-mesh method to generating hydrodynamic models for maneuvering simulation of two submerged bodies in relative motion. Journal of Computer Science and Cybernetics **27**(4), 353-362 (2011).
46. Leo, D.J.: Engineering Analysis of Smart Material Systems, vol. 1st Edition. John Wiley and sons Inc., Hoboken, New Jersey USA (2007)
47. LLC, m.: Nichrome 70-30 Medium Temperature Resistor Material. http://www.matweb.com/search/DataSheet.aspx?MatGUID=70c6833687d54cb4a000bd49ffd8e86c&ckck=1. 2018
48. Yip, M.C., Niemeyer, G.: High-performance robotic muscles from conductive nylon sewing thread. In: 2015 IEEE International Conference on Robotics and Automation (ICRA) 2015, pp. 2313-2318. IEEE

49. Tadesse, Y., Thayer, N., Priya, S.: Tailoring the response time of shape memory alloy wires through active cooling and pre-stress. Journal of Intelligent Material Systems and Structures **21**(1), 19-40 (2010).
50. Saharan, L., Tadesse, Y.: Robotic hand with locking mechanism using TCP muscles for applications in prosthetic hand and humanoids. In: Bioinspiration, Biomimetics, and Bioreplication 2016 2016, p. 97970V. International Society for Optics and Photonics
51. Inc., A.: Ansys Fluent. In. https://www.ansys.com/, (2018)
52. Shepherd, R.F., Ilievski, F., Choi, W., Morin, S.A., Stokes, A.A., Mazzeo, A.D., Chen, X., Wang, M., Whitesides, G.M.: Multigait soft robot. Proceedings of the National Academy of Sciences **108**(51), 20400-20403 (2011).
53. Zhang, F., Thon, J., Thon, C., Tan, X.: Miniature underwater glider: Design, modeling, and experimental results. In: 2012 IEEE International Conference on Robotics and Automation 2012, pp. 4904-4910. IEEE
54. Zhou, H., Hu, T., Xie, H., Zhang, D., Shen, L.: Computational and experimental study on dynamic behavior of underwater robots propelled by bionic undulating fins. Science China Technological Sciences **53**(11), 2966-2971 (2010).

Figures

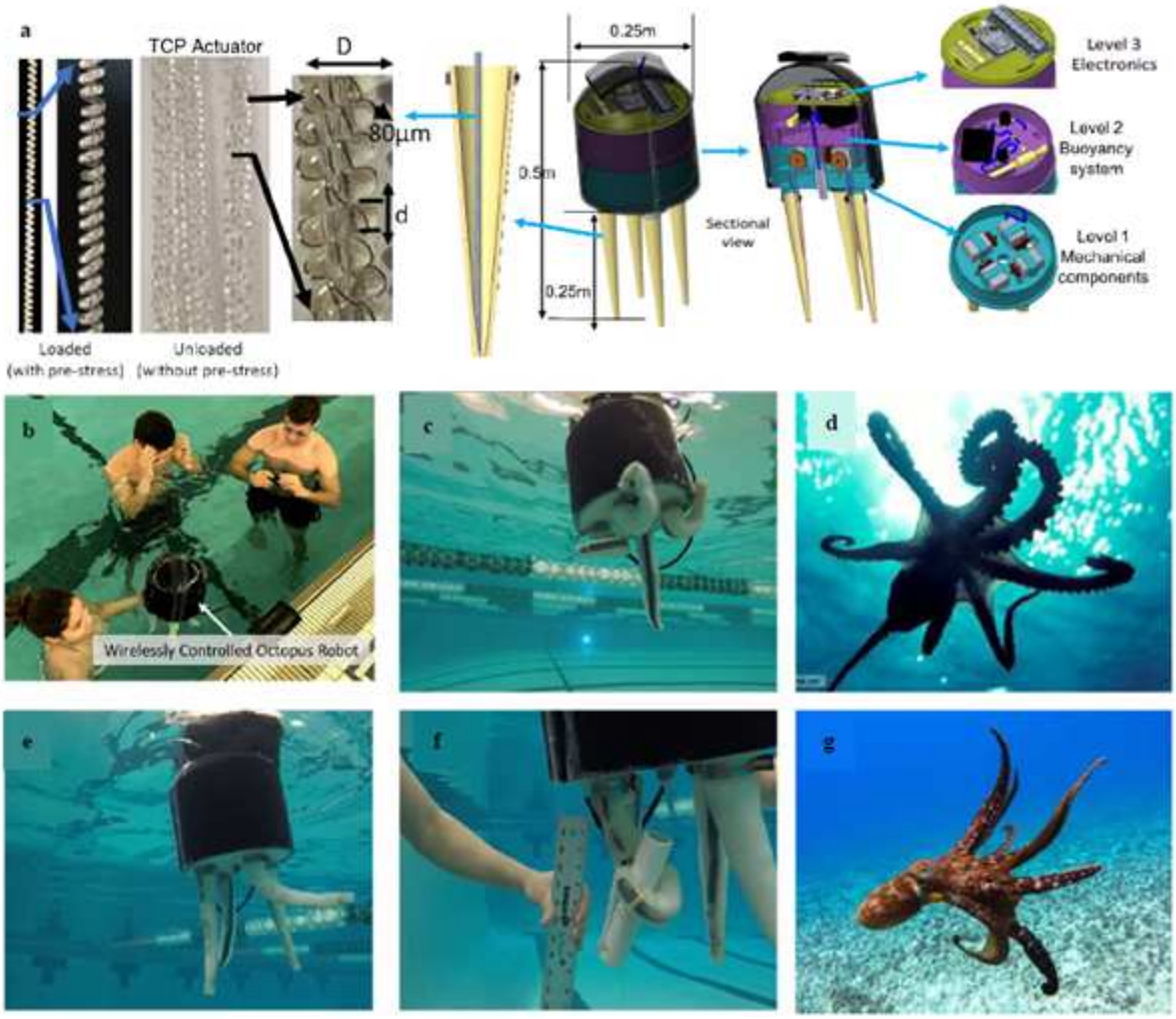

Figure 1

Kraken hybrid robot for underwater grasping. a TCP fishing line actuator in loaded and unloaded conditions after annealing, diameter, D = 2.80 mm. The resistance wire is Nichrome (nickel and chromium) with diameter, dw=80 µm. CAD model showing the major components of the hybrid robot, b Kraken deployed in water, c Curling 3 arms, d Octopus found in nature with curling tentacles, e Floating on the surface, f Grasping PVC pipe underwater, g Natural octopus swimming.

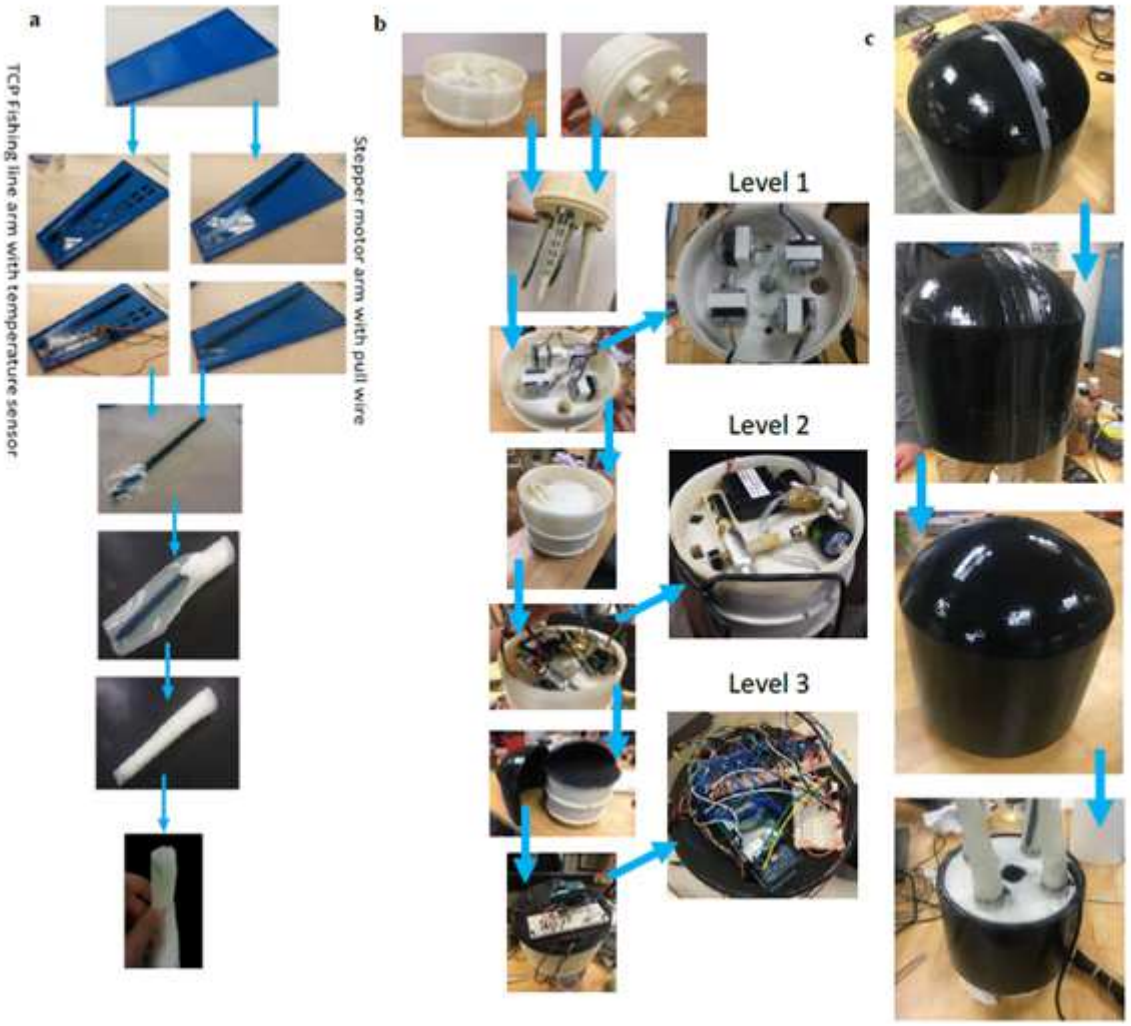

Figure 2

Fabrication process (a) Silicone arm fabrication process, (b) 3D printed parts assembly, detailed view of the three internal levels, level 1stepper motors, level 2 buoyancy system, level 3 electrical circuit. (c) Water sealing process using FlexSeal paint.

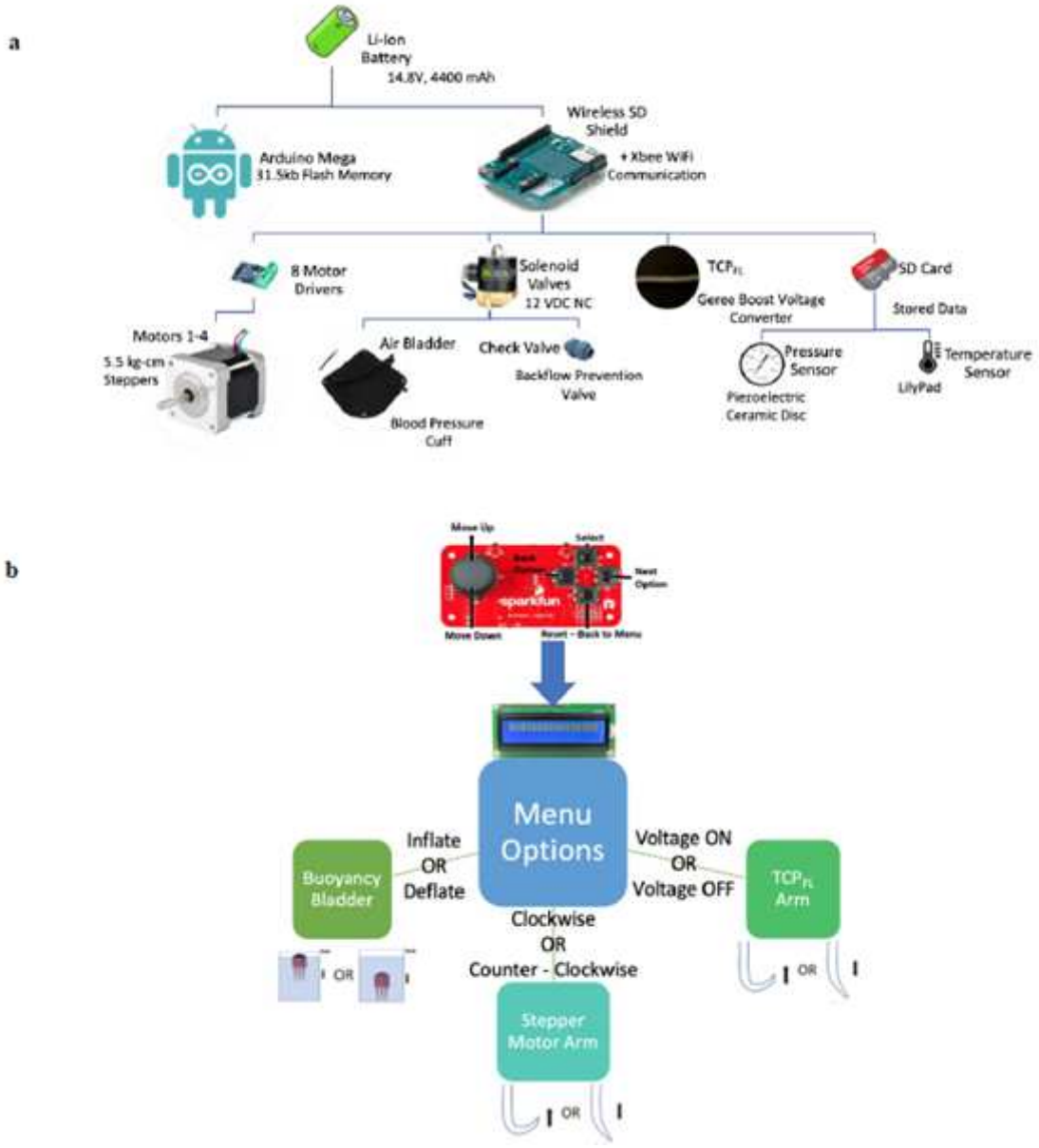

Figure 3

(a) Wiring component diagram with snapshot of the wireless controlling joystick, (b) Programed controlling menu command.

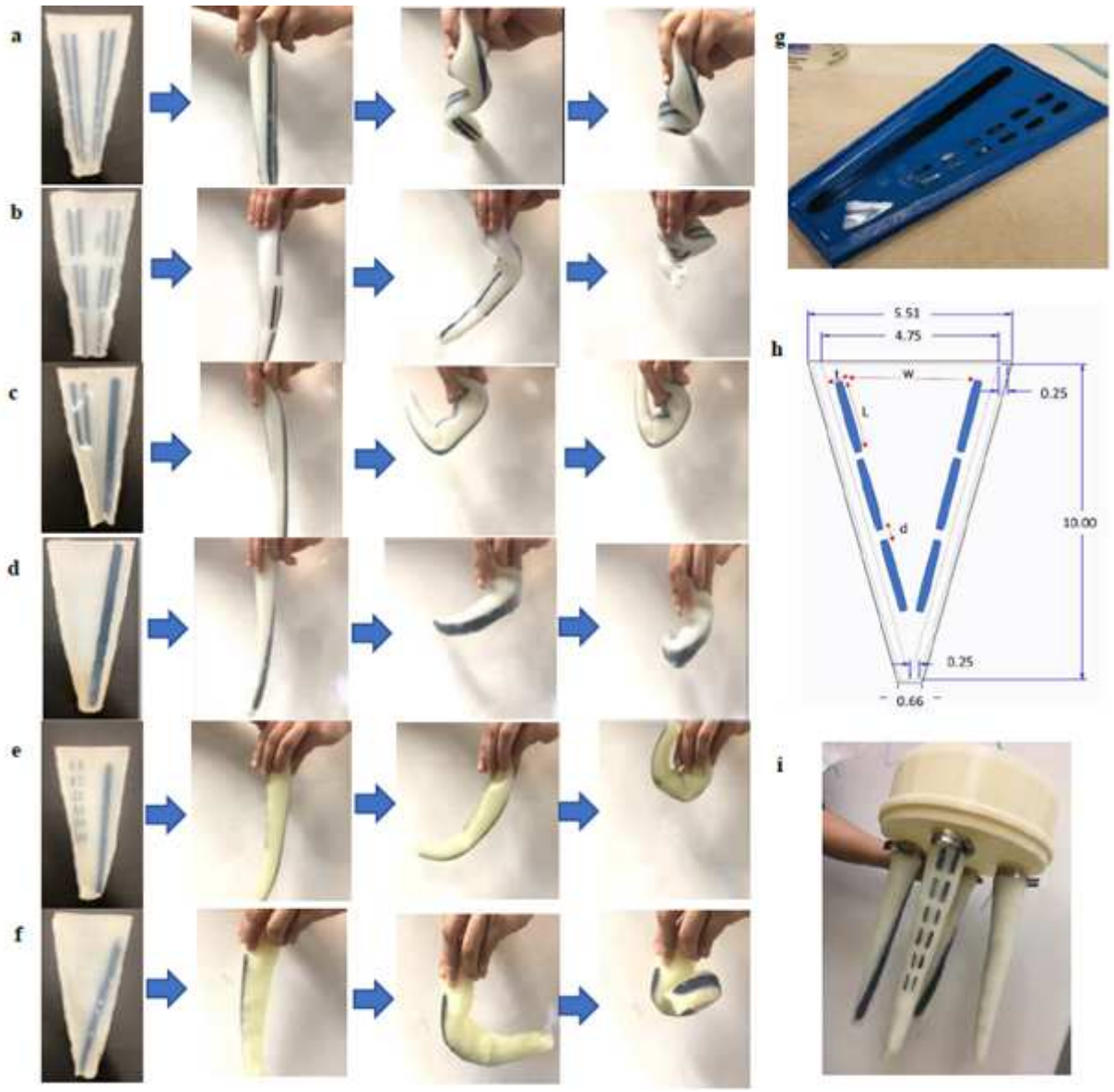

Figure 4

Different configuration of the octopus arm when spring steel, silicone and filler materials are changed: a Double full length with no filler(Type I), b Sectioned double full length with no filler(Type II), c Half length on one side and full length on the other side with no filler added(Type III), d Full length added on one side with no filler(Type IV), e Sectional half-length on one side and single full length on the other side with no filler added(Type V), f Single full length added diagonally with filler(Type VI). Molding method and assembly: g Sample of spring steel embedded in silicone, h A schematics of octopus arm mold in (inches). In the figure, t is the thickness of the spring steel, L is the length, d is the distance, n is the number of spring steels embedded, i Different arm configurations (Type II, IV,V,VI) mounted on the robotic structure.

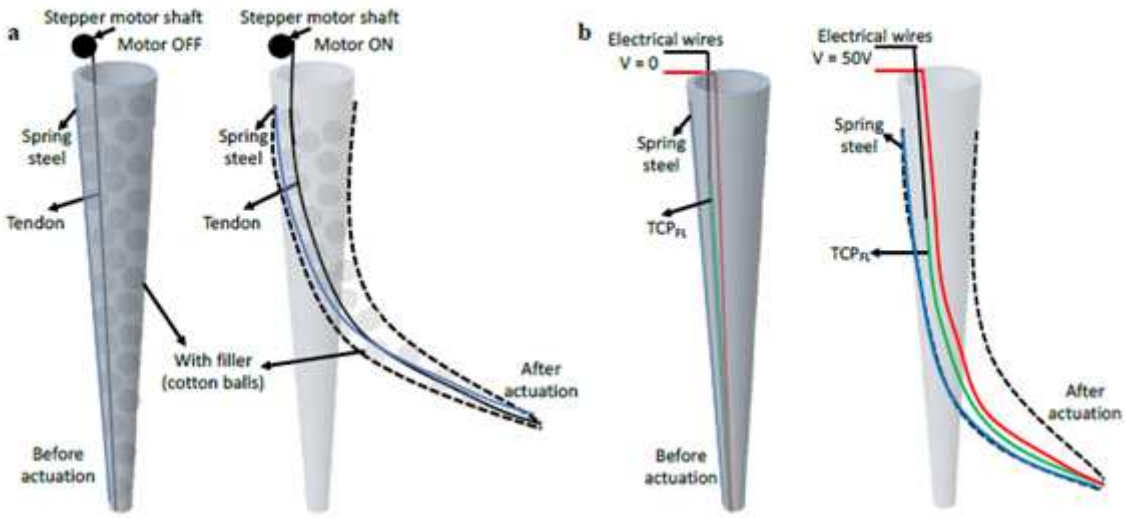

Figure 5

Schematics of the actuation mechanisms: a utilizing stepper motors and b utilizing TCPFL

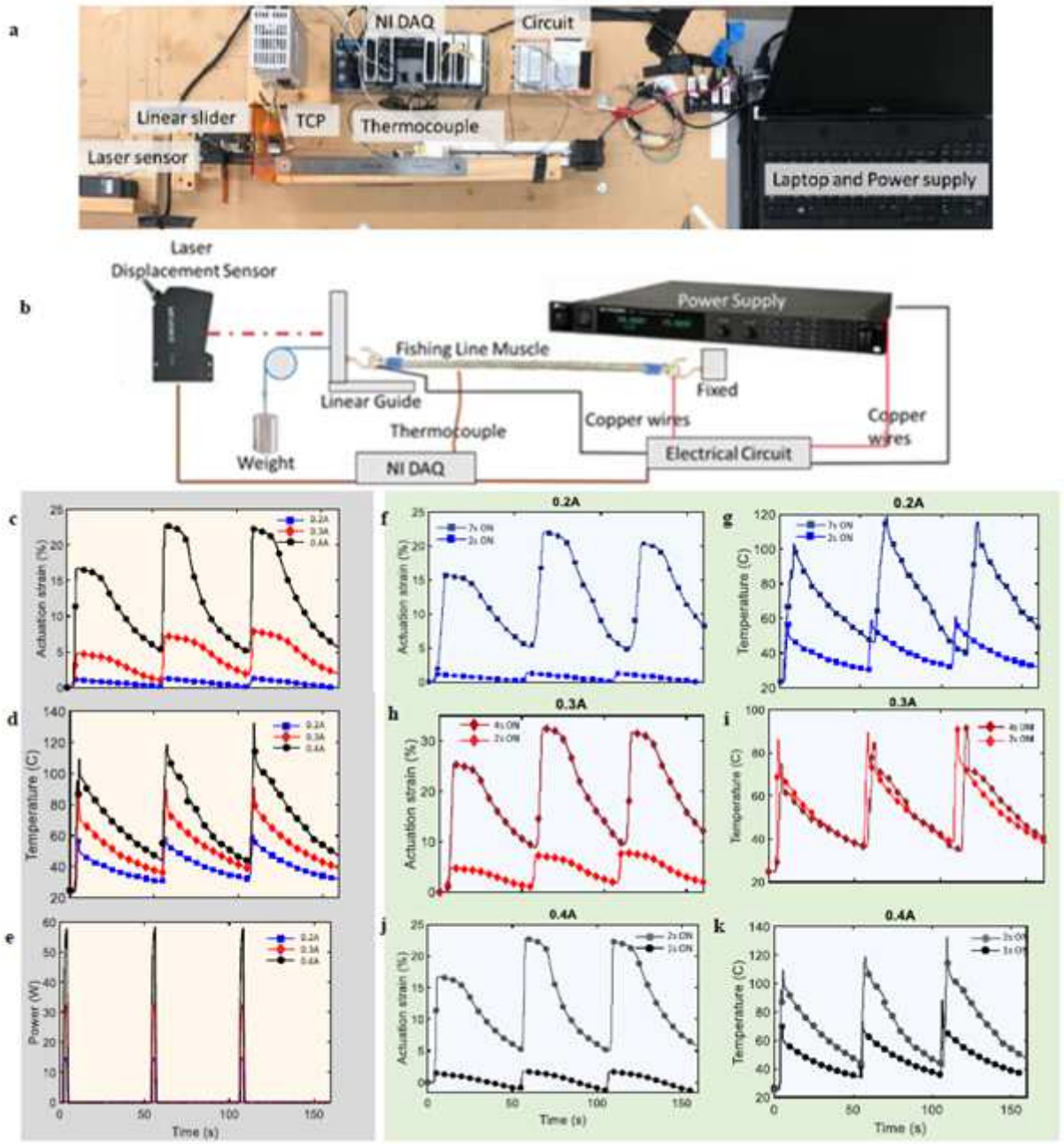

Figure 6

Experimental characterization of self-coiled with nichrome TCPFL actuator: a Isotonic test experimental set up, b Experimental schematics. Three cycles experimental results at 2s ON and 50s OFF for 0.2A,0.3A, and 0.4A input current: c Actuation strain, d Temperature, e Power, f&g Effect of heating time on actuation strain and temperature for 0.2A, h&i for 0.3A, j&k for and 0.4A. Markers are skipped at an increment of 50 data points.

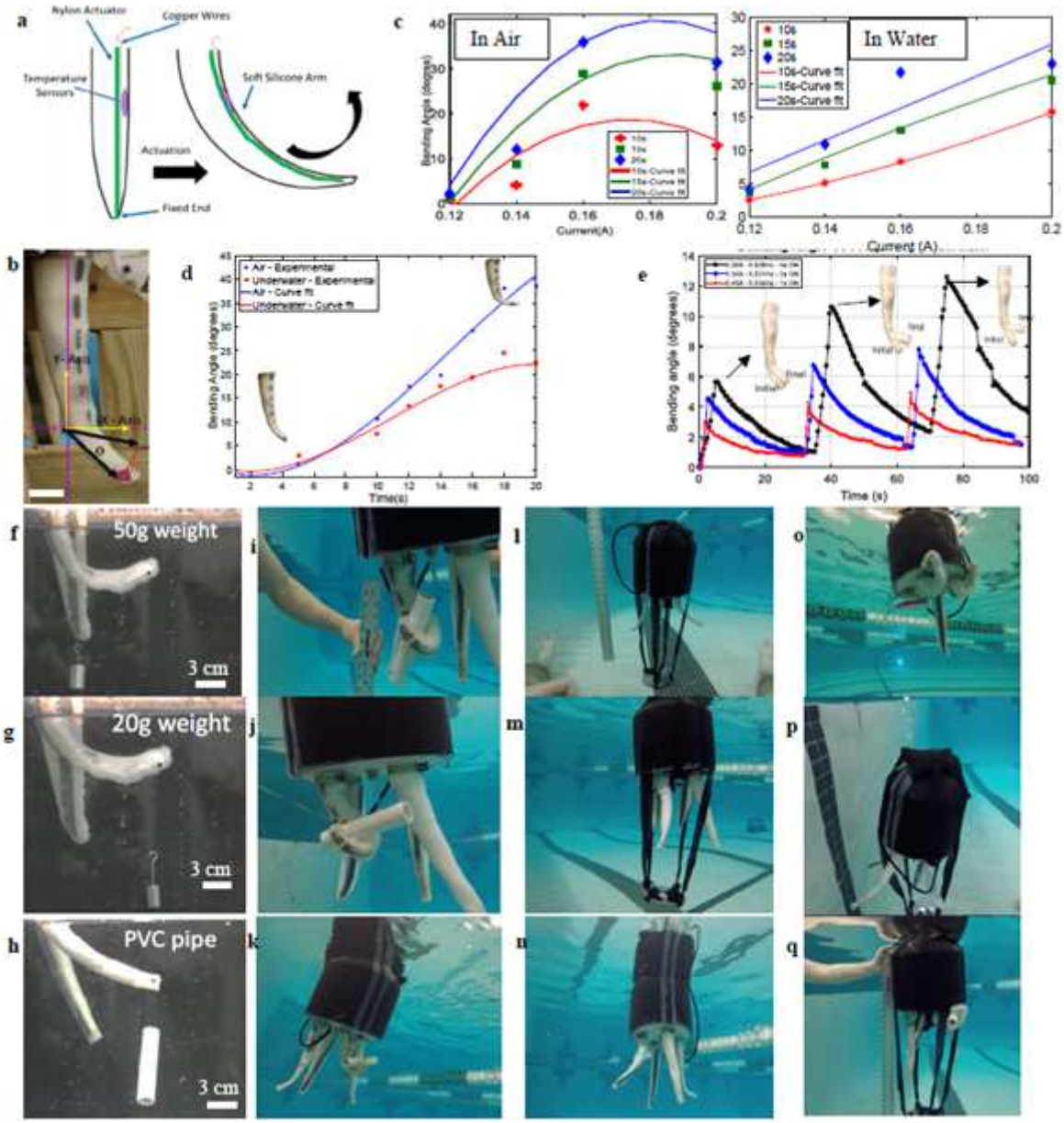

Figure 7

Charactrization of the Kraken arms.: a Schematics of the muscle connections (TCPFL length = 100mm), b TCP octopus arm showing bending angle, c Bending angle vs input current at different time points (left in air and right in the water), d Bending angle vs time at input current of 0.16A in air and in underwater condition. Tested in air and in underwater conditions, e Cyclic underwater actuation for low, medium, and high input current with variation of duty cycles. Experimental TCPFL silicone arm grasping objects in a 70-gallon fish tank: f-g 50g and 20g calibrated weight hanging on a wire, h Small PVC hooked on a wire. Kraken deployed in a swimming pool (depth 6ft) actuated by stepper motors: i,j,k Grapsing of PVC pipe, l,m,n Arms in resting position while carrying 2.5kg payload, o Curling of octopus arms, p Bouyancy system releasing air, robot sinking, q Floating while grasping PVC with 2.5kg payload

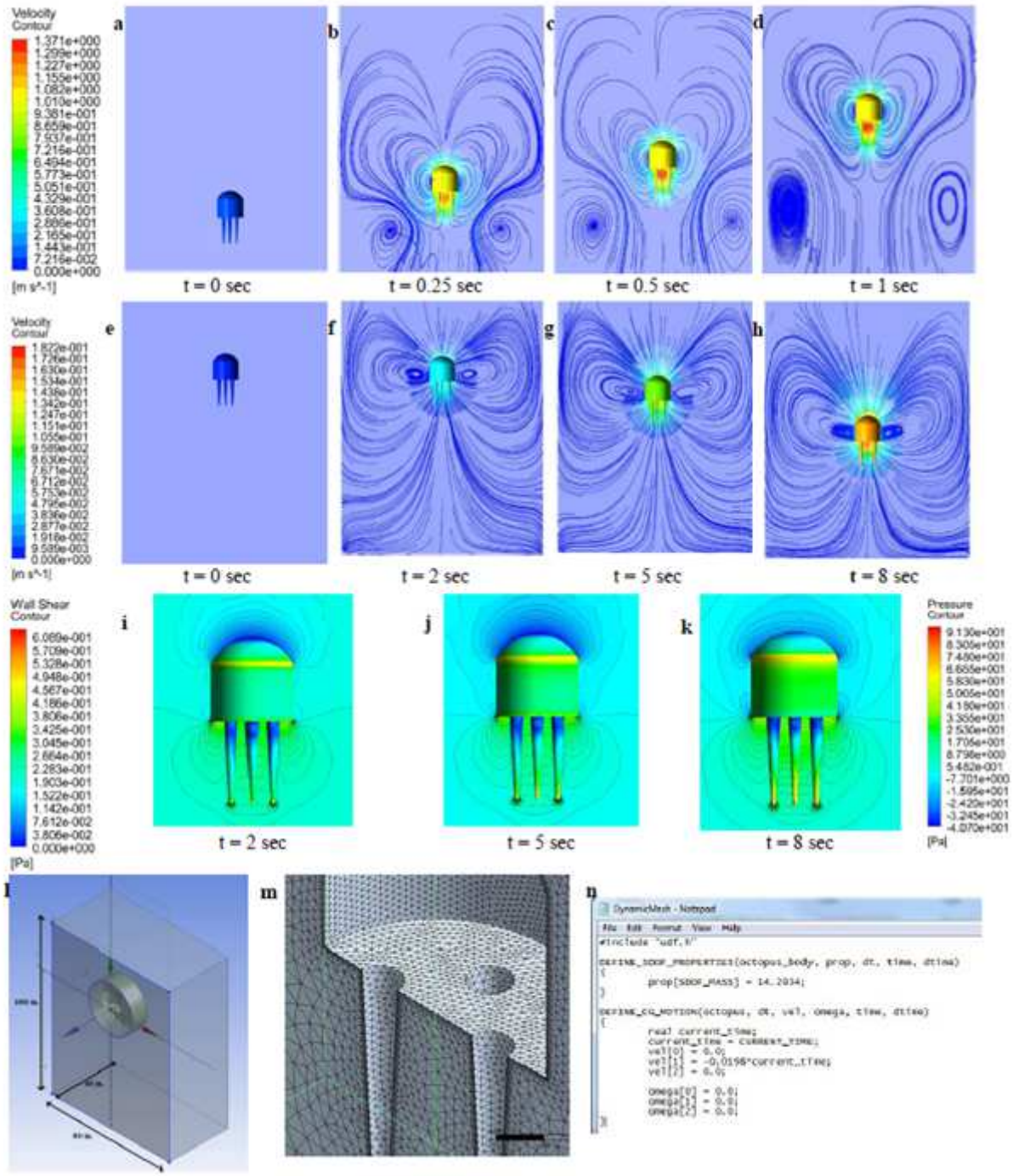

Figure 8

Flow simulation for Kraken: a-d Flow field generated around the Kraken moving up with constant speed of 1m/s at various times, e-h Flow field generated around the Kraken accelerating downwards at 0.0198 m/s2 at various times, i-k Pressure contours around and wall shear on surface of Kraken accelerating downwards at various times. l-n Simulation set up and mesh parameters in ansys fluid simulation

Supplementary Files

This is a list of supplementary files associated with this preprint. Click to download.

- SuppoctopusSep29YAOct16YAFinal.pdf